

# Efficient Holistic Control: Self-Awareness across Controllers and Wireless Networks

Ma, Yehan; Lu, Chenyang; Wang, Yebin

TR2020-002 January 08, 2020

## Abstract

Process automation is embracing wireless sensor-actuator networks (WSANs) in the era of Industrial Internet. Despite the success of WSANs for monitoring applications, feedback control poses significant challenges due to data loss and stringent energy constraints in WSANs. Holistic control adopts a cyber-physical system approach to overcome the challenges by orchestrating network reconfiguration and process control at run time. Fundamentally, holistic control leverages self-awareness across control and wireless boundaries to enhance the resiliency of wireless control systems. In this article, we explore efficient holistic control designs to maintain control performance while reducing the communication cost. The contributions of this work are five-fold: (1) We introduce a holistic control architecture that integrates low-power wireless bus (LWB) and two control strategies, rate adaptation and self-triggered control, specifically proposed to reduce communication cost; (2) We present two online rate selection approaches, namely, heuristic and optimal rate selections; (3) We design novel wireless network mechanisms to support rate adaptation and self-triggered control, respectively, in a multi-hop WSAN; (4) We build a real-time network-in-the-loop simulator that integrates MATLAB/Simulink and a three-floor WSAN testbed to evaluate wireless control systems; (5) We empirically explore the tradeoff between communication cost and control performance under alternative holistic control approaches. Our case studies show that rate adaptation and self-triggered control offer advantages in control performance and energy efficiency, respectively, in normal operating conditions. The advantage in energy efficiency of self-triggered control, however, may diminish under harsh physical and wireless conditions due to the cost of recovering from data loss and physical disturbances.

*ACM Transactions on Cyber-Physical Systems*

© 2020 MERL. This work may not be copied or reproduced in whole or in part for any commercial purpose. Permission to copy in whole or in part without payment of fee is granted for nonprofit educational and research purposes provided that all such whole or partial copies include the following: a notice that such copying is by permission of Mitsubishi Electric Research Laboratories, Inc.; an acknowledgment of the authors and individual contributions to the work; and all applicable portions of the copyright notice. Copying, reproduction, or republishing for any other purpose shall require a license with payment of fee to Mitsubishi Electric Research Laboratories, Inc. All rights reserved.



# Efficient Holistic Control: Self-Awareness across Controllers and Wireless Networks

YEHAN MA and CHENYANG LU, Washington University in St. Louis, USA

YEBIN WANG, Mitsubishi Electric Research Laboratories, USA

Process automation is embracing wireless sensor-actuator networks (WSANs) in the era of Industrial Internet. Despite the success of WSANs for monitoring applications, feedback control poses significant challenges due to data loss and stringent energy constraints in WSANs. *Holistic control* adopts a cyber-physical system approach to overcome the challenges by orchestrating network reconfiguration and process control at run time. Fundamentally, holistic control leverages self-awareness across control and wireless boundaries to enhance the resiliency of wireless control systems. In this article, we explore efficient holistic control designs to maintain control performance while reducing the communication cost. The contributions of this work are five-fold: (1) We introduce a holistic control architecture that integrates low-power wireless bus (LWB) and two control strategies, *rate adaptation* and *self-triggered control*, specifically proposed to reduce communication cost; (2) We present two online rate selection approaches, namely, heuristic and optimal rate selections; (3) We design novel wireless network mechanisms to support rate adaptation and self-triggered control, respectively, in a multi-hop WSAN; (4) We build a real-time network-in-the-loop simulator that integrates MATLAB/Simulink and a three-floor WSAN testbed to evaluate wireless control systems; (5) We empirically explore the tradeoff between communication cost and control performance under alternative holistic control approaches. Our case studies show that rate adaptation and self-triggered control offer advantages in control performance and energy efficiency, respectively, in normal operating conditions. The advantage in energy efficiency of self-triggered control, however, may diminish under harsh physical and wireless conditions due to the cost of recovering from data loss and physical disturbances.

CCS Concepts: • **Networks** → **Sensor networks**; • **Computer systems organization** → **Sensor networks**.

Additional Key Words and Phrases: industrial wireless control, multi-hop mesh network, network reconfiguration, network-in-the-loop simulation, cyber-physical systems, rate adaptation

## 1 INTRODUCTION

Wireless sensor-actuator networks (WSANs) are being adopted in industrial process automation for their advantages in reducing deployment and maintenance cost. While existing WSANs are usually used for monitoring, it remains challenging to support feedback control loops over WSANs, which is referred to as wireless networked control system (WNCS) [1]. First, compared with traditional networked control systems (NCSs) with wired networks, the control performance of WNCS can be compromised by data losses due to dynamic channel conditions in WSANs. This is largely unacceptable because control performance is closely related not only to the factory's profits, but also machine operator's safety and the environment. Second, a wireless device that requires a power cord is often impractical in industry settings (e.g., ABB [2] and Emerson [3]). In practice, an independent and reliable power supply – battery – is often mandatory, but with the disadvantage of their finite energy. Given the difficulty to replace batteries in harsh industrial environments, to ensure a reliable connection between the control center and the sensors and actuators despite the long distance, the key to the design of field devices and wireless standards (e.g. WirelessHART) is to maximize the battery life of the devices such that they could be battery powered for 4 to 10 years. Therefore, it is crucial to improve

---

Authors' addresses: Yehan Ma; Chenyang Lu, Washington University in St. Louis, St. Louis, MO, 63130, USA, {yehan.ma,lu}@wustl.edu; Yebin Wang, Mitsubishi Electric Research Laboratories, Cambridge, MA, 02139, USA, yebinwang@ieee.org.

---

© 2018 Association for Computing Machinery.

Manuscript submitted to ACM

1

the energy efficiency of WSANs while maintaining control performance in a WNCS. Finally, WNCS must be resilient to both disturbance to the physical plant and external interference to the wireless networks. Therefore, a practical and dependable industrial WNCS must meet the following requirements: (1) *control performance*, which brings economic benefits; (2) *energy efficiency*, which reduces maintenance cost; and (3) *resiliency*, which prevents accidents.

Traditionally, the wireless network and the physical process are managed separately in a WNCS at run time. The lack of coordination between network and plant management forces conservative designs that trade energy for control performance. For example, a WNCS may rely on high sampling rates to guarantee control performance under worst-case conditions, even though the same sampling rates may result in excessive communication cost under normal conditions. Conversely, a less conservative design may result in a fragile system vulnerable to physical disturbance and/or wireless interference. In contrast to the traditional approach, the *holistic control* approach aims to enhance the resiliency and efficiency of WNCS by *cojoining* network reconfiguration and process control [4].

In this work we explore efficient holistic control designs to maintain control performance at low energy cost. We develop holistic control approaches that incorporate two alternative strategies, *rate adaptation (RA)* and *self-triggered control (ST)*. We note that RA introduces adaptation in a traditional *time-driven* control framework, while ST is a representative *event-driven* control approach. Exploring both strategies in holistic control allow us to investigate the design tradeoff involved in holistic control design. Specifically, the contributions of this work are five-fold.

- We introduce a new *holistic control architecture* that integrates multi-hop wireless networks running the Low-power Wireless Bus (LWB) protocol and two alternative control strategies, RA and ST;
- We present two online RA approaches based on heuristics and optimal rate selections, respectively, and establish stability of the resultant closed-loop control system;
- We design *robust network adaptation* mechanisms to support RA and ST, respectively, in multi-hop LWB networks;
- We build *RT-WCPS*, a real-time network-in-the-loop simulator that integrates MATLAB/Simulink and a physical WSAN testbed to evaluate wireless control systems;
- We empirically explore the tradeoff between communication cost and control performance under alternative holistic control approaches.

Our case studies show that RA and ST offer advantages in control performance and energy efficiency, respectively, in normal operating conditions. The advantage in energy efficiency of ST, however, may diminish under harsh physical and wireless conditions due to the cost of recovering from data loss and physical disturbance.

The rest of the article is organized as follows: Sec. 2 reviews related works on WNCS designs. Sec. 3 introduces the system architecture of holistic control systems. Secs. 4 and 5 detail the control and network designs of RA and ST. Sec. 6 presents the real-time wireless cyber-physical simulator (RT-WCPS), and Sec. 7 analyzes the experimental results.

## 2 RELATED WORK

WNCSs comprise distributed sensors, actuators, and controllers communicating through wireless networks. Due to the benefits of flexibility and low deployment and maintenance cost, WNCSs are expanding their applications over industry processes, autonomous warehouses and smart factories [5]. However, WNCSs face serious challenges due to the inherent dynamics in wireless conditions and limited energy resources in wireless networks [6]. The problem of resilient and efficient wireless control has been investigated in the fields of control theory, wireless networks, and more recently network-control co-designs [1].

105 In control theory, state observers [7] (e.g., extended Kalman filter) have been introduced to handle packet loss and  
106 communication latency in WNCSS. To reduce communication cost, aperiodic control has been proposed as an alternative  
107 to periodic control. Examples include event-triggered control [8, 9] and self-triggered control [10]. However, existing  
108 implementation of aperiodic control was based on a single-hop wireless network [11] instead of the multi-hop WSANs  
109 that are widely adopted in process industries due to their flexibility and scalability in industrial environments. Supporting  
110 aperiodic control on a multi-hop WSAN is challenging because industrial WSAN standards usually employ TDMA  
111 protocols for predictable communication. The aperiodic communication triggered by aperiodic control is incompatible  
112 with the periodic, time-driven nature of communication in industrial multi-hop WSANs.  
113

115 In wireless networks, given the latency, packet delivery, and energy consumption bounds by control designers,  
116 network designs can achieve optimized energy-efficiency [12], reliability [13], load balancing [14], and real-time  
117 performance [15] under various wireless channel conditions and network topologies. Breath [12] is proposed to  
118 minimize the energy cost while ensuring a desired packet delivery rate and delay of the WSAN by adjusting routing,  
119 MAC, radio power and sleeping discipline. SchedEX [13] is proposed to minimize delay while providing reliability  
120 guarantees by producing the TDMA schedule. QU-RPL [14] achieves load balancing and improves end-to-end reliability  
121 based on queue utilization. Blink [15] supports hard real-time communication in multi-hop WSAN at low energy cost.  
122 However, few of those protocols are cognizant of control performance directly. Better network performance does not  
123 always imply good control performance of the physical plant. Indeed, the internal properties of the physical plant, such  
124 as its stability, inherently influence the impact of improvements in network communication on control performance.  
125

126 Recent effort on network-control co-design aims to jointly optimize the network and control at design time. Previous  
127 works on sampling rate optimization [16–20] exploit the freedom of sampling rates to optimize control performance  
128 under various network protocols and system settings. For wired control, Li et al. [16] minimize useful information  
129 loss under network bandwidth constraints. Our project differs from this work in the objective of optimizing control  
130 performance while lowering energy cost of WSAN. Goswami et al. [17] handle both real-time and control performance  
131 constraints by modeling ECUs over a FlexRay bus. While the work is based on a wired network, FlexRay shares  
132 similarities to LWB used in our system in their TDMA-based scheduling approach. Our project differs from the work in  
133 our focus on online rate adaptation, while Goswami et al. tackled the optimization problem of offline optimization.  
134 Furthermore, we also address self-triggered control approaches and network adaptation protocols.  
135

136 For wireless control, Demirel et al. [18] design packet forwarding policies over an unreliable and energy-constrained  
137 WSAN; Saifullah et al. [19] optimize sampling rates under the end-to-end deadline constraints of data flows in a  
138 WirelessHART mesh network; Kim et al. [20] focus on control over IEEE 802.11 networks. Asymmetric routing [21]  
139 enhances control performance and network efficiency by applying different routing strategies to sensing and actuation  
140 data flows since sensing and actuation can have different levels of robustness to packet loss. However, all these efforts  
141 focus on offline designs instead of online adaptation, which limits the resiliency and efficiency of WNCSS operating in  
142 dynamic conditions (e.g., under network interference and physical disturbance; under transient state or steady state).  
143 Online rate optimization has been investigated in [22–24] for different objectives. Specifically, Bai et al. [22] minimize  
144 tracking error under the constraints of network capacity and delay requirement; Bao et al. [23] optimize the control  
145 performance over noisy channels under total bit-rate constraint; Colandairaj et al. [24] adapt sampling rates using a  
146 static sampling policy based on control performance and network performance in an IEEE 802.11b network.  
147

148 This article considers the energy cost of WSANs, and the design and implementation of the network reconfiguration  
149 mechanisms for RA over a multi-hop WSAN under the LWB protocol, which are not addressed by these previous  
150 works. In prior work [4], we proposed the concept of holistic control that co-joins network management and physical  
151

control at run time. As a simple proof of concept, we presented a holistic control example that adjusts the numbers of transmissions (TxS) based on physical states. In this article, we generalize the designs of holistic control by incorporating more sophisticated control approaches, namely RA and ST. The new control approaches require more sophisticated network reconfiguration mechanisms that are both efficient and robust. Furthermore, the alternative control approaches (time-driven vs. event-driven) allow us to explore the design tradeoff involved holistic control in multi-hop WSNs.

It is challenging to conduct experiments on industrial control systems in the field, especially under cyber and physical disturbances. Lab-scale equipment, on the other hand, is usually too small for realistic cyber-physical experiments, particularly for multi-hop wireless networks. Therefore, simulation tools are of vital importance to WNCs. Truetime [25] is a MATLAB/Simulink-based tool, which enables simulations of CPU scheduling, communication and control algorithms. NCSWT [26] integrates MATLAB/Simulink and NS-2 for modeling and simulation of NCSs. Neither of the native wireless simulations of Truetime nor the NS-2 simulator can accurately model the probabilistic and irregular packet receptions of WSNs [27, 28]. WCPS [29] integrates MATLAB/Simulink and TOSSIM [30] specifically designed to emulate complex temporal link dynamics of WSNs. However, given the complexity of wireless communication in physical environments, simulators cannot always capture the real-world behavior of WSNs. Network-in-the-loop simulations have recently been developed to address the limitation of wireless simulations by incorporating physical wireless networks [31]. Experiments presented in [11] integrate two double-tank systems with a single-hop wireless network. Baumann et al. [32–34] integrate two real inverted pendulums and a 13-node multi-hop WSN testbed, achieving sampling rates of tens of millisecond. However, the physical plants in laboratory settings used in those experiments cannot represent large-scale industrial processes and are limited to the specific lab-scale physical plants. In this work, we design and implement a general network-in-the-loop simulator which integrates MATLAB/Simulink simulations and a 70-node WSN testbed.

### 3 WIRELESS CONTROL SYSTEM ARCHITECTURE

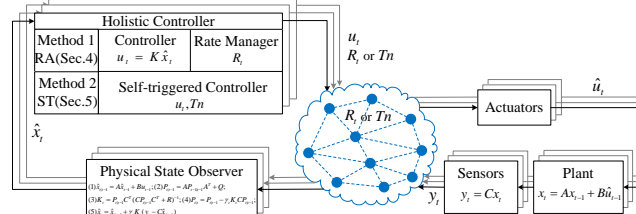


Fig. 1. Holistic WNCs architecture.

Fig. 1 depicts the holistic wireless control architecture. The holistic controllers (1) control the physical plants by communicating with sensors and actuators through a multi-hop WSN, and (2) reconfigure the WSN based on control needs at run time. Multiple control loops share the same WSN. As shown in Fig. 1, at time  $t$ , a sensor sends its measurements  $y_t$  to a remote holistic controller over the multi-hop WSN. A state observer [7] estimates the state of the plant. Based on the estimated state  $\hat{x}_t$ , the holistic controller generates both (1) the control commands ( $u_t$ ) and (2) the network reconfiguration signal ( $R_t$  or  $T_n$ ). Two instances of holistic controller, namely RA and ST, are introduced. For RA (or ST), the control commands  $u_t$  and the updated sampling rate  $R_t$  (or next event time  $T_n$ ) generated by the holistic controller are sent to the WSN through flooding. For the control commands, the actuator receives  $u_t$  and applies  $\hat{u}_t$  to the physical plant. If  $u_t$  fails to be delivered by the deadline, the actuator reuses the control input received in the last period,  $\hat{u}_{t-1}$ . For network reconfiguration, every node in the network reconfigures its communication schedule based on  $R_t$  or  $T_n$ . The details of control and network designs for RA and ST are presented in Sec. 4 and Sec. 5, respectively.

### 3.1 Physical control system

In this article, control design and analysis are performed for the physical plant which can be modelled as a linear time-invariant system (LTI) as follows

$$x_{t+1} = Ax_t + Bu_t, y_t = Cx_t, \quad (1)$$

where  $t$  is the time index,  $x_t \in \mathbb{R}^n$  is the state vector,  $u_t \in \mathbb{R}^m$  is the input vector,  $y_t \in \mathbb{R}^p$  is the output vector,  $A \in \mathbb{R}^{n \times n}$ ,  $B \in \mathbb{R}^{n \times m}$ , and  $C \in \mathbb{R}^{p \times n}$ . We assume that the pair  $(A, B)$  is controllable and that the pair  $(A, C)$  is observable. This implies the existence of a linear state feedback controller  $u_t = Kx_t$  which renders the closed-loop control system asymptotically stable. Note that the proposed wireless network reconfiguration mechanisms however are not limited to LTI systems, and are applicable to nonlinear and time-varying systems.

The stability analysis of the resultant control system can be conducted by using the Lyapunov theory. System (1) is stable if there exists a positive definite Lyapunov function [35]

$$V(x_t) = x_t^\top P x_t, \quad (2)$$

such that

$$V(x_{t+1}) - V(x_t) = x_t^\top ((A + BK)^\top P (A + BK) - P) x_t = -x_t^\top Q x_t, \quad (3)$$

where  $P, Q$  are positive definite matrices. In other words,  $P$  and  $Q$  satisfy the discrete-time Lyapunov equation:

$$(A + BK)^\top P (A + BK) - P = -Q. \quad (4)$$

### 3.2 Wireless sensor-actuator network

**3.2.1 Low-Power Wireless Bus (LWB).** The WSAN extends the LWB [36] protocol to support data communication and network reconfiguration for holistic control. LWB is based on *Glossy* [37], a fast-flooding protocol that exploits the constructive interference among concurrent transmissions of radios compatible with the IEEE 802.15.4 standard. The flooding process is entirely driven by radio events, i.e., a transmission is triggered by completing a packet reception, which drastically speeds up the process and provides microsecond-level WSAN synchronization. Under LWB, nodes take turns to flood their packets in a time-triggered fashion using Glossy flooding according to a single global schedule. A sink node is responsible for disseminating the schedule to all the nodes in the network. Thus, the multi-hop many-to-all communication can be regarded as a single communication resource (shared bus) that runs on a single clock [15].

Adopting LWB as the underlying communication protocol brings significant benefits. Thanks to Glossy flooding, communication in LWB is topology independent. Besides, LWB is a wireless protocol that provides deterministic end-to-end latency given a global schedule [36], which largely simplifies the analysis of system stability over the multi-hop WSAN. Additionally, fast Glossy flooding achieves propagation latency within 10 ms over 100 nodes (8 hops, 3 TxS). We can take the advantage to realize fast network reconfiguration by quickly flooding network configurations across the entire network, an important feature as network reconfiguration is a key element of holistic control.

**3.2.2 Implicit scheduling of multi-rate LWB.** Unlike prior work [15] which uses a centralized scheduler node to operate scheduling algorithms, we tailored LWB for implicit scheduling. All nodes schedule themselves based on information from holistic controllers, such as flooding rates or next event timers of each control loop. We define a data flow of WSAN as  $f_{i,j}$ , which transmits data from a source node  $s_{i,j}$  to a destination node  $d_{i,j}$ , where  $i \in \{1, 2, \dots, n\}$  is the control loop index, and  $j \in \{1, 2, \dots, m_i\}$  is the flow index of the control loop  $i$  ( $l_i$ ). Accordingly,  $n$  is the number of control loops, and  $m_i$  is the number of data flows in  $l_i$ . For example, the control loop  $l_1$  has two data flows  $f_{1,1}$  and  $f_{1,2}$ ,

among which  $f_{1,1}$  is a sensing flow transmitting measurements from a sensor node ( $s_{1,1}$ ) to a controller node ( $d_{1,1}$ ), and  $f_{1,2}$  is an actuation flow transmitting control command from a controller node ( $s_{1,2}$ ) to an actuator ( $d_{1,2}$ ). A MIMO control loop can have multiple sensing and actuation flows. The update rate of control commands in the control loop  $l_i$  is denoted as  $R_i$ . The operation period of  $l_i$  is  $T_i = \frac{1}{R_i}$ . We assume the rates of the flows in one control loop are equal.

In implicit scheduling of data flows, each node stores a static global schedule of all data flows, denoted by entries  $f_{i,j}[s_{i,j}, d_{i,j}, t_{i,j}]$ ,  $t_{i,j}$  is the relative time slot reserved for flow  $f_{i,j}$  in LWB period  $T = \frac{1}{R}$ . LWB operates at the highest rate of all the control loops,  $R = \max_{1 \leq i \leq n} R_i$ . Fig. 2 shows a simple static schedule. We assume there are three control loops and each loop has one flow. All loops have same rate  $R_1 = R_2 = R_3 = \frac{1}{T}$ . Thus, the rate of LWB is  $R = \frac{1}{T}$ . Therefore, we get the static schedule entries:  $f_{1,1}[2, 1, 1]$ ,  $f_{2,1}[3, 4, 2]$ ,  $f_{3,1}[4, 1, 3]$ . In each period  $T$ , the synchronization message  $S$  is flooded by the sink node in the beginning of every period, followed by three data slots assigned for three flows.

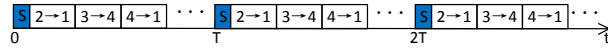


Fig. 2. LWB with static global schedule. ( $f_{1,1}$ , node2  $\rightarrow$  node1,  $\frac{1}{T}$  Hz;  $f_{2,1}$ , node3  $\rightarrow$  node4,  $\frac{1}{T}$  Hz;  $f_{3,1}$ , node4  $\rightarrow$  node1,  $\frac{1}{T}$  Hz.)

This static schedule is calculated assuming each control loop runs at its highest candidate rate. The static schedule can be calculated offline using any scheduling algorithm, e.g., EDF or RM. In practice, industrial process control systems usually run at sampling rates lower than 1 Hz [38]. By adopting fast Glossy flooding (flooding a packet over 100 nodes within 10 ms [37]), WSA can guarantee the schedulability of tens of data flows, which suggests the feasibility of the static schedule. We refer interested readers to [15, 39] for network designs with tighter real-time requirements.

To implement multi-rate LWB using implicit scheduling, besides the static global schedule, the only information that all nodes need are the rates of all the control loops  $R_i$ . In order to make the *implicit scheduling* work properly, the potential  $T_i$  of all the loops should be set to integral multiples of the shortest period  $T$ . Then each node can independently decide whether to flood  $f_{i,j}$  or sleep at  $t_{i,j}$  within the time interval  $[(k-1)T, kT]$ ,  $k = 1, 2, 3, \dots$ , depending on  $R_i$ . Fig. 3 shows an example of the *implicit scheduling* with the static schedule in Fig. 2, where  $R_1 = \frac{1}{T}$ ,  $R_2 = \frac{1}{2T}$ , and  $R_3 = \frac{1}{4T}$ . All nodes flood  $f_{1,1}$  at the first data slot of every period  $T$ , flood  $f_{2,1}$  at the second data slot every other period  $T$ , and flood  $f_{3,1}$  at the third data slot every  $4T$ . They sleep at the rest blank data slots.

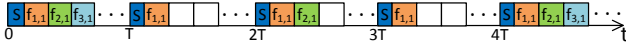


Fig. 3. Implicit scheduling. ( $f_{1,1}$ , node2  $\rightarrow$  node1,  $\frac{1}{T}$  Hz;  $f_{2,1}$ , node3  $\rightarrow$  node4,  $\frac{1}{2T}$  Hz;  $f_{3,1}$ , node4  $\rightarrow$  node1,  $\frac{1}{4T}$  Hz.)

In implicit scheduling, since each node stores the static schedule, the network reconfiguration commands can be generated by any source nodes in WSA distributively, in contrast to *centralized scheduling* in which the whole schedule is sent by the sink in the beginning of each period  $T$ . We will present how network reconfiguration signals, such as  $R_i$ , are disseminated in Sec. 4.2 and 5.2.

### 3.3 Holistic management

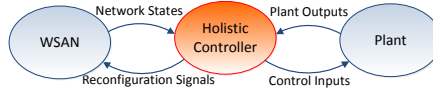


Fig. 4. Holistic management of WNCSS.

As shown in Fig. 4, we develop a holistic control architecture that bridges the gap between the plant control and WSA management. Based on the current status of physical plants and WSA, the holistic controller generates two kinds of commands at the same time, one for dynamically adjusting the network configuration, and the other for operating the physical plants. In the following two sections, we focus on two specific efficient holistic control designs: rate adaptation and self-triggered control over a multi-hop mesh network.



**ALGORITHM 1:** Heuristic rate adaptation algorithm for loop  $i$ 


---

**Input:**  $x_t, t, \tau, t_0 = t, \lambda$ , candidate rates (ascending):  $\{R_{i,1}, R_{i,2}, \dots, R_{i,s}\}$ , current  $R_i = R_{i,j}, A_i, B_i, K, P, Q$   
**Output:** updated  $R_i$

Calculate  $V(x_t)$  as defined in (2), and  $V_{Dth}, V_{Ith}$ ;  
**if**  $V(x_t)$  remains below  $V_{Dth}$  for a time interval of  $\tau$ , **and**  $R_i > R_{i,1}$  **then**  
 $R_i \leftarrow R_{i,j-1}$ ; //  $R_i$  decreases  
**else if**  $V(x_t) > V_{Ith}$  **and**  $R_i < R_{i,s}$  **then**  
**if** last rate adaptation is a decrease **then**  
 $t_0 \leftarrow t; R_i \leftarrow R_{i,j+1}$ ; //  $R_i$  increases  
**if** last rate adaptation is an increase **and**  $V(x_t) > (1 - \frac{\beta}{\alpha_2})^{t-t_0} V(x_{t_0})$  **then**  
 $t_0 \leftarrow t; R_i \leftarrow R_{i,j+1}$ ; // succeeding  $R_i$  increases  
**else**  
 $R_i$  remains constant

---

**4 RATE ADAPTATION**

The data flow rates of a WSA have direct impacts on control performance and energy cost. The higher the rates, the better the control performance, but the higher the energy cost [18]. In this section, in order to ensure the control performance while reducing the network energy cost, we adjust the rates of the WSA based on control performance during runtime. We introduce the holistic controller design and the network design of rate adaptation (RA).

**4.1 Control design**

We propose two online RA strategies. First is a heuristic-based RA which selects rate based on physical states and customized thresholds. Second is an optimal RA by minimizing a certain performance metric characterizing the control performance and communication cost. Finally, the stability of the resultant closed-loop control system is established. Please note that, in this paper, the sampling rate of multiple loops are adapted in a distributed way. That is, each loop has its own holistic controller. Each loop determines its own sampling rate ( $R_i$ ) individually. The rate is calculated and potentially adapted every sampling period. We discuss the RA strategies for loop  $i$  in this section.

**4.1.1 Heuristic rate adaptation.** We employ a similar adaptation algorithm proposed in [4] (Alg. 1). The value of the Lyapunov function  $V(x_t)$  in (2), the metric of the control performance, provides the bounds of the state error. Given (2),

$$\alpha_1 \|x_t\|^2 \leq V(x_t) \leq \alpha_2 \|x_t\|^2, \quad (5)$$

where  $\alpha_1$  and  $\alpha_2$  are the smallest and largest eigenvalues of  $P$ , respectively. The value of  $V(x_t)$  is used to update the rate. Given a customized state error bound, denoted as  $se = \|x_{se}\|^2$ , we set the rate increasing threshold  $V_{Ith} = \alpha_1 \|x_{se}\|^2$ . Based on (5), we have  $\|x_t\|^2 \leq \|x_{se}\|^2$ , if  $V(x_t) \leq V_{Ith}$ . Furthermore, we adopt a more stringent decreasing threshold  $V_{Dth}$  to indicate that the system performs well,  $V_{Dth} = \lambda \alpha_1 \|x_{se}\|^2, \lambda \in (0, 1)$ . If  $V(x_t)$  remains below  $V_{Dth}$  for a customized time interval  $\tau$ , the control system is regarded in good condition. Given (3),

$$V(x_{t+1}) - V(x_t) \leq -\beta \|x_t\|^2, \quad (6)$$

where  $\beta$  is the smallest eigenvalue of  $Q$ . Given (5) and (6), we can get the upper bound of the ideal Lyapunov function, described by (7). We set this upper bound as the trigger of succeeding rate increases.

$$V(x_{t+j}) \leq (1 - \beta/\alpha_2)^j V(x_t). \quad (7)$$

The heuristic RA algorithm of a holistic controller is presented in Alg. 1, and its complexity is  $O(1)$ .

4.1.2 *Optimal rate adaptation.* A disadvantage of the aforementioned heuristics-based RA is that it requires hand tuning that can be challenging for complex control systems. Furthermore, it does not offer a systematic way to balance control system performance and communication cost, the two important and conflicting concerns in wireless control systems. Henceforth, we formulate rate selection as an optimization problem. The objective of the optimization problem is to minimize a cost function that incorporates both control performance and communication cost.

As described in Sec. 3.2.2, each candidate period of a feedback control loop is an integral multiple of the smallest sampling period  $T$ . Let  $T_s = n_s T$  be the least common multiple of all candidate periods of a feedback control loop. In order to compare the control performance resulting from different rates, we rewrite all possible systems with different sampling rates in the slowest time frame  $T_s$  in a process referred to as *lifting* [40].

By lifting the system in the slowest time frame  $T_s$ , the system is given by

$$x_{t+n_s T} = A_{d1}^{n_s} x_t + \begin{bmatrix} A_{d1}^{n_s-1} B_{d1} & \dots & B_{d1} \end{bmatrix} \begin{bmatrix} u_{t,1} \\ \vdots \\ u_{t+(n_s-1)T,1} \end{bmatrix} \quad (8)$$

where  $u_{t+iT,1}$  is the control input during time interval  $[t+iT, t+(i+1)T)$ , and  $A_{d1} = e^{A_c T}$ ,  $B_{d1} = \int_0^T e^{A_c(T-\tau)} B_c d\tau$ , where  $A_c$  and  $B_c$  are the system matrices of the original continuous system dynamics  $\dot{x} = A_c x + B_c u$ . For the lowest sampling rate  $1/T_s$ , the corresponding system does not need lifting and has the dynamics

$$x_{t+n_s T} = A_{dn_s} x_t + B_{dn_s} u_{t,n_s} \quad (9)$$

where  $u_{t,n_s}$  is defined over  $[t, t+n_s T)$ , and  $A_{dn_s} = e^{n_s A T}$ ,  $B_{dn_s} = \int_0^{n_s T} e^{A(n_s T-\tau)} B d\tau$ . To make a fair evaluation for systems resultant from different rates, we rewrite the slowest system (9) as follow

$$x_{t+n_s T} = A_{dn_s} x_t + \begin{bmatrix} A_{d1}^{n_s-1} B_{d1} & \dots & B_{d1} \end{bmatrix} \begin{bmatrix} u_{t,n_s} \\ \vdots \\ u_{t+(n_s-1)T,n_s} \end{bmatrix} = A_{d1}^{n_s} x_t + \sum_{i=0}^{n_s-1} A_{d1}^i B_{d1} u_{t,n_s} \quad (10)$$

where  $u_{t,n_s} = u_{t+iT,n_s}$ ,  $i \in \{0, \dots, n_s - 1\}$ , and  $A_{dn_s} = A_{d1}^{n_s}$ . Finally we can rewrite the system dynamics of loop  $i$ , depending on the rate  $R_i$ , as follows

$$x_{t+n_s T} = \begin{cases} A_{d1}^{n_s} x_t + \sum_{i=1}^{n_s-1} A_{d1}^i B_{d1} u_{t+iT,1}, & \text{if } R_i = 1/T \\ \vdots \\ A_{d1}^{n_s} x_t + \sum_{i=1}^{n_s-1} A_{d1}^i B_{d1} u_{t+iT,k}, & \text{if } R_i = 1/(kT) \\ \vdots \\ A_{d1}^{n_s} x_t + \sum_{i=1}^{n_s-1} A_{d1}^i B_{d1} u_{t,n_s}, & \text{if } R_i = 1/T_s \end{cases} \quad (11)$$

Based on (11), the states and inputs of systems with all candidate rates are lifted to the lowest rate. We are now ready to formulate rate selection as an optimization problem. Let us evaluate the cost function over a horizon of  $N$  sample periods corresponding to the lowest sample rate, i.e., the horizon for performance evaluation lasts  $NT_s$  seconds. Since each loop can select its rate individually, we can formulate  $n$  independent optimization problems, where  $n$  is the number of feedback control loops. Coordination between different control loops is part of our future work. The optimization problem for loop  $i$  has decision variables of an  $N$ -dimensional vector  $R_i(k)$ , where its  $k$ th element  $R_i(k)$  represents the sample rate during the time interval  $[t + (k-1)T_s, t + kT_s)$ . Finally, the cost function is defined as a

weighted combination of control performance and communication cost:

$$\mathcal{J}(x_t, \mathbf{R}_i) = \sum_{j=0}^{N-1} \{x_{t+jT_s}(\mathbf{R}_i(j))^\top W_Q x_{t+j}(\mathbf{R}_i(j)) + \epsilon_1 u_{t+j}(\mathbf{R}_i(j))^\top W_R u_{t+j}(\mathbf{R}_i(j)) + \epsilon_2 \mathbf{R}_i(j)\}, \quad (12)$$

where  $x_{t+j}$  is predicted based on (11) given  $x_t$  and control law,  $x_{t+j}(\mathbf{R}_i(j))^\top W_Q x_{t+j}(\mathbf{R}_i(j)) + \epsilon_1 u_{t+j}(\mathbf{R}_i(j))^\top W_R u_{t+j}(\mathbf{R}_i(j))$  represents control performance including state cost and control cost,  $W_Q, W_R$  set relative weights of state deviation and control effort,  $x_{t+j}$  denotes  $x_{t+jT_s}$ , and

$$u_{t+j} = \begin{cases} [u_{t+jT_s,1}, \dots, u_{t+jT_s+(n_s-1)T,1}]^\top, & \text{if } \mathbf{R}_i(j) = 1/T \\ \vdots \\ [u_{t+jT_s,n_s}, \dots, u_{t+jT_s+(n_s-1)T,n_s}]^\top, & \text{if } \mathbf{R}_i(j) = 1/T_s. \end{cases}$$

In (12), the communication cost is linearly proportional to sampling rate  $\mathbf{R}_i(j)$ . Constant  $\epsilon_1$  is to weight state error versus control cost, and  $\epsilon_2$  is to weight control performance versus communication cost. When  $\epsilon_2$  approaches 0, which means that network energy cost is ignored, the WNCS is prone to stay at the fastest sampling rate to achieve better control performance. We define this scenario as *cheap network* in analogy with *cheap control*, which is the case  $W_R = 0$  [41] when evaluate control performance. As a result, the optimization problem of loop  $i$  can be written as follows

$$\underset{\mathbf{R}_i}{\text{minimize}} \quad \mathcal{J}(x_t, \mathbf{R}_i) \quad (13a)$$

$$\text{subject to} \quad \mathbf{R}_i = [\mathbf{R}_i(1), \dots, \mathbf{R}_i(N)], \text{ with } \mathbf{R}_i(k) \in \{\mathbf{R}_{i,1}, \dots, \mathbf{R}_{i,s}\} \quad (13b)$$

$$x_{t+j} = \begin{cases} A_{d1}^{n_s} x_{t+j-1} + \sum_{i=1}^{n_s-1} A_{d1}^i B_{d1} u_{t+(j-1)T_s+iT,1}, & \text{if } \mathbf{R}_i(j) = 1/T \\ \vdots \\ A_{d1}^{n_s} x_{t+j-1} + \sum_{i=1}^{n_s-1} A_{d1}^i B_{d1} u_{t+(j-1)T_s,n_s}, & \text{if } \mathbf{R}_i(j) = 1/T_s \end{cases} \quad (13c)$$

$$u_t = Kx_t. \quad (13d)$$

The optimization problem (13) has  $N$  integer decision variables. Since the decision variables  $\mathbf{R}_i(j)$  belongs to a finite set of candidate rates, the optimal rate adaptation problem is an integer programming problem, which could be computationally expensive to solve at every sampling period. To reduce the computational complexity, we simplify (13) by assuming that the control system stays at the same rate over the horizon, i.e.,  $\mathbf{R}_i(1) = \dots = \mathbf{R}_i(N) = \mathbf{R}_i$ . Accordingly, the cost function is given by

$$\mathcal{J}(x_t, R_i) = \sum_{j=0}^{N-1} \{x_{t+jT_s}(R_i)^\top W_Q x_{t+j}(R_i) + \epsilon_1 u_{t+j}(R_i)^\top W_R u_{t+j}(R_i) + \epsilon_2 R_i\}. \quad (14)$$

The simplified optimization problem takes the following formulation

$$\underset{R_i}{\text{minimize}} \quad \mathcal{J}(x_t, R_i) \quad (15a)$$

$$\text{subject to} \quad R_i \in \{R_{i,1}, \dots, R_{i,s}\}. \quad (15b)$$

$$x_{t+j} = \begin{cases} A_{d1}^{n_s} x_{t+j-1} + \sum_{i=1}^{n_s-1} A_{d1}^i B_{d1} u_{t+(j-1)T_s+iT,1}, & \text{if } R_i = 1/T \\ \vdots \\ A_{d1}^{n_s} x_{t+j-1} + \sum_{i=1}^{n_s-1} A_{d1}^i B_{d1} u_{t+(j-1)T_s,n_s}, & \text{if } R_i = 1/T_s \end{cases} \quad (15c)$$

$$u_t = Kx_t. \quad (15d)$$

Although the simplified optimization problem (15) is an integer programming problem, for each loop  $i$  it has only one scalar decision variable  $R_i$  (instead of  $N$  in (13)). Furthermore, the number of candidate rates is usually small in practice, which significantly reduces the computation complexity. We solve the optimization problem by brute force search. Note that the system matrixes of rate lifting can be calculated offline. Given a horizon of  $N$ ,  $M$  candidate rates, and  $n_s = \frac{T_s}{T}$ , the computation complexity is  $O(MNn_s)$ . We also evaluate the computation cost in MATLAB/Simulink on a 2.5 GHz Intel Core i7 processor. The settings of the experiments are the same as in Sec. 7.2.2 ( $n_s = 2^{M-1}$ ). Fig. 5 shows the execution time of solving (15) for 2000 times. As shown in Fig. 5A, with candidate rates  $M = 3$ , the median and worst-case execution time when horizon  $N < 25$  is below 1 ms and 2.1 ms, respectively. As shown in Fig. 5B, with  $N = 10$ , the median and worst-case execution time when  $M \leq 6$  is below 4 ms and 11 ms, respectively. The execution time is negligible compared with the 1 s sampling period. These results show that the problem (15) is online solvable.

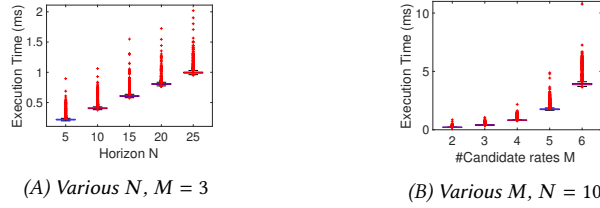


Fig. 5. Execution time of solving (15) with various horizon  $N$  and number of candidate rates  $M$ .

REMARK 4.1. Since we target industrial process control systems with sampling rates lower than 1 Hz [38], we tailor the rate selection for our WSA design with an assumption of the existence of “worst-case-guaranteed” schedule in Sec. 3.2. Hence there is no network resource/schedulability constraint, and the rate selections of multiple loops can be done individually.

For systems with schedulability constraints, we can provide schedulability guarantee by generalizing the optimal RA problems (13) and (15) to incorporate schedulability constraints. We replace the objective function in [19] Eq.(8) by  $\sum_{i=1}^n \mathcal{J}(x_t, \mathbf{R}_i)$  and adding system dynamic constraints (11) of all loops. Since we apply LWB, as studied in [15], the real-time scheduling constraints can be simplified from multi-processor task scheduling in [19] to uni-processor case. However, given that the configuration space of the corresponding centralized optimization problem is much larger than (13) and (15), and the introduce of schedulability constraints, the resultant optimization problem can be computationally expensive to solve online. In addition, this approach requires centralized management of the control loops. Extending our work to consider schedulability constraint is part of future work.

4.1.3 *Stability analysis.* Deploying the aforementioned RA algorithms renders the closed-loop control system being a switched system, whereas the switch is governed by the RA algorithm. Since it is difficult, if not impossible, to formulate the analytic formula of the switching sequence, we borrow the stability result for switched systems with arbitrary switching. Stability analysis tools for switched systems can be found in [42] and references therein. This work performs stability analysis and control design based on a well-received result: if there exists a common Lyapunov function for all subsystems, then the stability of the switched system is guaranteed under arbitrary switching. It is revealed that the construction of such a common Lyapunov function among all candidate rates can be formulated as a Linear Matrix Inequality (LMI) problem: solves for  $P$  satisfying

$$(A(R_i) + B(R_i)K)^T P (A(R_i) + B(R_i)K) - P < 0, \quad \forall R_i \in \{R_{i,1}, \dots, R_{i,s}\} \quad (16)$$

where  $A(R_i)$  and  $B(R_i)$  are discretized system matrices of loop  $i$  corresponding to the sample rate  $R_i$ . If there is a feasible solution for the LMI problem (16), then  $V(x_t) = x_t^T P x_t$  is the common Lyapunov function of all candidate rates, and the stability is established.

The aforementioned stability analysis, in a deterministic setting, provides a strategy to search for a common Lyapunov function  $V(x_t)$  that is used in Sec. 4.1.1. As described in Sec. 3.2.1, the latency bound of LWB is deterministic [36, 37]. In our test cases, the latency is shorter than one sampling period. Stability analysis under network latency of below one sampling period is well studied. We refer interested readers to [32, 43]. The stability analysis can be generalized to take indeterministic network latency and packet loss into account, which consequently leads to stochastic stability. Stability analysis under different network scenarios has been intensively studied in control community, and are not the focus of this article. We refer interested readers to stability analysis addressing network latency [43, 44] and packet loss with different distribution patterns [45, 46]. Despite the simplifications, our stability analysis provides practical guidance towards balancing the closed-loop control performance and network rate in real-world scenarios involving network latency and packet loss, as shown in case studies under network and physical interference in Secs. 7.4-7.6.

REMARK 4.2. *The existence of a single common Lyapunov function (16) for all candidate rates is a conservative but easy-to-check stability condition. The relaxation of conservativeness has been intensively studied in control community, and leads to numerous results [47–49]. For example, work [47] proposed to replace the single common Lyapunov function with a switched Lyapunov function, and established a sufficient condition of stability as stated in the following theorem.*

THEOREM 4.3 ([47], THM. 4). *If there exist symmetric matrices  $S(R_i)$ , matrices  $G(R_i)$  and  $U(R_i)$  such that  $\forall (R_i, R_j)$*

$$\begin{bmatrix} G(R_i) + G(R_i)^T - S(R_i) & (A(R_i)G(R_i) + B(R_i)U(R_i))^T \\ A(R_i)G(R_i) + B(R_i)U(R_i) & S(R_j) \end{bmatrix} > 0 \quad (17)$$

then the gain of state feedback control

$$K(R_i) = U(R_i)G(R_i), \forall R_i \in \{R_{i,1}, \dots, R_{i,s}\} \quad (18)$$

stabilizes the system.

The results in [47] shows the tradeoff between a single Lyapunov function for simplicity and a switched Lyapunov function that is less conservative but numerically hard to check.

## 4.2 Network reconfiguration

In this section, we present a run-time RA protocol for a mesh WSN. Packet loss has non-negligible impacts on WNCS, especially in the process of network reconfiguration. In the end of this section, we discuss packet loss recovery of RA.

4.2.1 *Candidate rates selection.* Sec. 4.1 considers how to adjust the rate of each loop. The candidate rates are also important design factors. To ensure that the rate transient processes work properly, the potential rates of each loop need to be designed intentionally. First, according to Sec. 3.2.2, when the offline scheduler schedules data flow  $f_{i,j}$ , it reserves time slots for fastest rate  $R$ . Second, the candidate periods of all the loops should be integral multiples of the shortest period  $T = \frac{1}{R}$ . Third, to ensure that the RA works properly with packet loss recovery, which will be discussed later in Sec. 4.2.3, the candidate rates of each loop should be harmonic, e.g.,  $(\frac{1}{T}, \frac{1}{2T}, \frac{1}{4T})$  or  $(\frac{1}{T}, \frac{1}{3T}, \frac{1}{9T})$ . Schedule examples for candidate rates of  $(\frac{1}{T}, \frac{1}{2T}, \frac{1}{4T})$  are shown in Table 1. A filled unit indicates that a packet is sent in that time slot. In addition, according to Sec. 4.1.3, in order to guarantee stability, a common Lyapunov function should exist by solving the LMI problem formulated by subsystems induced by all candidate rates.

4.2.2 *Network reconfiguration based on piggyback.* The holistic controller of  $l_i$  adopts a *piggyback* mechanism to disseminate a newly computed  $R_i$  for data flows  $f_{i,j}, j = 1, 2, \dots, m_i$ . The holistic controller of  $l_i$  piggybacks  $R_i$  with the

Table 1. Schedule examples for loop 1 with candidate rates of  $R_{1,1} = \frac{1}{T}$  Hz,  $R_{1,2} = \frac{1}{2T}$  Hz,  $R_{1,3} = \frac{1}{4T}$  Hz

Rate	$t_{1,1}$	$t_{1,1} + T$	$t_{1,1} + 2T$	$t_{1,1} + 3T$	$t_{1,1} + 4T$	$t_{1,1} + 5T$	$t_{1,1} + 6T$	$t_{1,1} + 7T$	$t_{1,1} + 8T$	$t_{1,1} + 9T$
$R_{1,1} = \frac{1}{T}$ Hz	█	█	█	█	█	█	█	█	█	█
$R_{1,2} = \frac{1}{2T}$ Hz	█		█		█		█		█	
$R_{1,3} = \frac{1}{4T}$ Hz	█			█			█			█

Table 2. Packet loss recovery for rate adaptation of flow  $f_{11}$

	$t_{1,1}$	$t_{1,1} + T$	$t_{1,1} + 2T$	$t_{1,1} + 3T$	$t_{1,1} + 4T$	$t_{1,1} + 5T$
Updated rate $R_i$	$R_{1,1}$	$R_{1,2}$	$R_{1,2}$	$R_{1,2}$	$R_{1,2}$	$R_{1,2}$
Node 2*	$R_{1,1}(1)$	$R_{1,1}(1) \rightarrow R_{1,2}$	$R_{1,2}(1)$	$R_{1,2}(/)$	$R_{1,2}(1)$	$R_{1,2}(/)$
Node 3	$R_{1,1}(1)$	$R_{1,1}(1) \rightarrow R_{1,2}$	$R_{1,2}(1)$	$R_{1,2}(/)$	$R_{1,2}(1)$	$R_{1,2}(/)$
Node 4	$R_{1,1}(1)$	$R_{1,1}(0)$	$R_{1,1}(1) \rightarrow R_{1,2}$	$R_{1,2}(/)$	$R_{1,2}(1)$	$R_{1,2}(/)$

actuation command. Therefore the data field of the actuation packet is  $[l_i, R_i, \text{Data}_i]$ . Because of the flooding nature of LWB, all nodes in the network can receive this update. Once a node receives an updated  $R_i$ , it will calculate a new schedule based on  $R_i$ , as described in Sec. 3.2.2.

The distributed network reconfiguration based on piggyback has several benefits over the conventional centralized network reconfiguration. First, this piggyback mechanism helps reduce energy cost by utilizing existing actuation data flows, saving the time and energy needed to calculate and deliver the whole schedule in every period. Second, the network reconfiguration commands can be flooded by any source nodes in WSAN distributively, in contrast to *centralized scheduling*, in which the whole schedule should be sent by the sink. In addition, implicit and distributed scheduling using piggyback is more reliable than a centralized scheduler. Packet loss in implicit scheduling affects only one loop, but the packet loss of centralized scheduling can affect all data flows.

**4.2.3 Packet loss recovery.** If a node loses the packet with the updated rate of  $l_i$ , it will use the current  $R_i$  until another packet of  $l_i$  is received. Therefore, it is possible that, at the same time, different nodes along the route of a flow are using different rates. Nevertheless, it is still possible for nodes to eventually receive the update. The transmissions of three nodes in Table 2 represent an example of packet loss recovery for flow  $f_{1,1}$  (source  $s_{1,1}$  is node 2), when a holistic controller updates the rate from  $R_{1,1}$  to  $R_{1,2}$  at the second period ( $t_{1,1} + T$ ).  $\{1, 0, /\}$  in brackets following  $R_{1,j}$  indicate that the node receives a packet, loses a packet, and remains sleeping, separately, correspond to schedule of  $R_{1,j}$  as shown in Table 1. In this example, the update rate is received by nodes 2 and 3, but fails to arrive at node 4 within the second period ( $t_{1,1} + T$ ) due to packet loss. Hence, the rates of nodes 2 and 3 switch to  $R_{1,2}$ , while node 4 continues to use  $R_{1,1}$ . Although node 4 use different rate, it is still possible for it to receive update rate in the third period ( $t_{1,1} + 2T$ ), since relative slot  $t_{1,1}$  in the third period is the common slot shared by  $R_{1,1}$  and  $R_{1,2}$ . If all candidate rates are harmonic, i.e., share as many common slots as possible, as described in Sec. 4.2.1, the node will recover faster from packet loss.

## 5 SELF-TRIGGERED CONTROL

Self-triggered control (ST) [10], an aperiodic event-driven control design, improves the efficiency of the network. The first single-hop wireless network protocol for aperiodic control is presented in [11]. However, due to the lack of network protocol, aperiodic control designs have not been adopted in multi-hop mesh networks. In this section, we respectively introduce control design and network design of ST.

### 5.1 Control design

In event-triggered control, trigger condition is checked in every sampling period. The time of actuation event cannot be known in advance, which requires the network to reserve resource for unknown events. The ST relaxes this requirement by predicting the future events based on system models. Intuitively, ST triggers sensing and actuation events only when

certain control performance is predicted to be lost. The self-triggered strategy we present in this article is motivated by [11]. Since a decreasing Lyapunov function  $V(x_t) = x_t^\top P x_t$  is the certificate of stability ( $P$  is achieved in Sec. 4.1.3), the desired control performance is defined by a decreasing function  $S(x_t)$ , upper bounding the evolution of Lyapunov function  $V(x_t)$ :  $V(x_t) \leq S(x_t)$ . Provided that  $V(x_t) \leq S(x_t)$  holds and  $S(x_t)$  is decaying over time, the closed-loop system is stabilized [10, 11]. The predicted time of the next sensing and actuation events is  $t_k = \min\{t > t_{k-1} | V(x_t) - S(x_t) \geq 0\}$ . Here, we adopt a feasible decreasing  $S(x_t)$ , as follows:

$$S(x_t) = V(x_{t_{k-1}}) e^{-\gamma V(x_{t_{k-1}})^\delta (t - t_{k-1})}. \quad (19)$$

We induce the term  $\gamma V(x_{t_{k-1}})^\delta$ ,  $\gamma, \delta > 0$ , which makes the decreasing rate of  $S(x_t)$  adapt to the value of the Lyapunov function (state error). That is, when  $V(x_{t_{k-1}})$  is large, which indicates severe state error, the  $S(x_t)$  decreases faster. Therefore, the sensing and actuation events are more likely to be triggered. On the other hand, when  $V(x_{t_{k-1}})$  is small, which indicates the current states are close to equilibrium point, the  $S(x_t)$  decreases slower. The sensing and actuation events are unnecessary and less likely to be triggered.

Please note that unlike event-triggered control, the trigger condition of which is checked in every sampling period, self-triggered control checks the trigger condition based on predictions based on system model, which makes it less resilient to disturbance. In order to provide robustness guarantees of the self-triggered control, an upper bound of the inter-transmission interval should be customized based on [11, 50, 51].

## 5.2 Network protocol for self-triggered control

### 5.2.1 Self-triggered transmissions.

Due to the predictive nature of ST, the network knows *a priori* when the event will be triggered by the holistic controllers. Therefore, nodes know the next time when they should wake up and flood data. Within the inter-transmission interval, the nodes sleep. In this way, the energy costs of nodes can be reduced compared with periodic control at the highest rate.

Similar to the network protocol of RA, the holistic controller uses the piggyback mechanism to disseminate a newly computed time of next transmission  $Tn_i$  for all data flows of  $l_i$ . Again,  $Tn_i$  should be integral multiples of  $T$ . The holistic controller piggybacks  $Tn_i$  with the actuation command. Therefore the data field of the actuation packet is  $[l_i, Tn_i, \text{Data}_i]$ . Because of flooding, all nodes in the network can receive this update. In a node, each data flow has an event timer. Once a node receives a  $Tn_i$ , it will set the value of  $\text{Timer}_{i,j}$  to  $Tn_i$  and start counting down from the next period. If the  $\text{Timer}_{i,j}$  expires, the node will wake up and flood in the pre-assigned relative slots  $t_{i,j}$  within  $T$ . Fig. 6 shows an example of self-triggered transmissions based on LWB. At the first period,  $f_{2,1}$  is flooded, and node 3, which is the source of  $f_{2,1}$ , receives and floods  $Tn_2 = 3T$  at slot that is assigned for  $f_{2,1}$ . Therefore, the next  $f_{2,1}$  is reserved and transmitted  $3T$  later at the fourth period. At the second period,  $f_{1,1}$  and  $f_{3,1}$  are transmitted, and  $Tn_1 = T$ ,  $Tn_3 = 2T$ , respectively. Therefore, the next  $f_{1,1}$  is reserved and transmitted at the third period, and  $f_{3,1}$  at the fourth period.

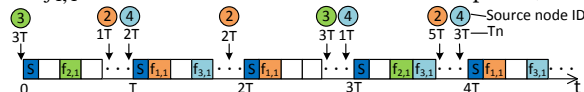


Fig. 6. Self-triggered transmission based on LWB ( $f_{1,1}$ , node2  $\rightarrow$  node1;  $f_{2,1}$ , node3  $\rightarrow$  node4;  $f_{3,1}$ , node4  $\rightarrow$  node1).

### 5.2.2 Why not event-triggered transmissions.

We adopt ST instead of event-triggered control. In event-triggered control, trigger conditions are checked every sampling period. Source node is aware of whether the event is triggered in current period, and it does not flood if the trigger condition is not violated. However, other nodes in mesh WSN do not know the trigger time in advance, they still wake up and keep listening in case certain events are triggered in current period.



Table 3. Impact of packet loss on self-triggered control of flow  $f_{1,1}$ 

	$t_{1,1}$	$t_{1,1} + T$	$t_{1,1} + 2T$	$t_{1,1} + 3T$	$t_{1,1} + 4T$	$t_{1,1} + 5T$
Updated inter-transmission time: $Tn_1$	$T$	$2T$		$2T$		$2T$
Node 2*	$2T(1) \rightarrow T$	$T(1) \rightarrow 2T$	$2T(/)$	$2T(1)$	$2T(/)$	$2T(1)$
Node 3	$2T(1) \rightarrow T$	$T(1) \rightarrow 2T$	$2T(/)$	$2T(1)$	$2T(/)$	$2T(1)$
Node 4	$2T(0)$	$2T(/)$	$2T(0)$	$2T(/)$	$2T(0)$	$2T(/)$

Therefore, event-trigger control systems over a multi-hop mesh network cannot reduce duty cycle of the network. As shown in Fig. 7, at the first period, the source node of  $f_{2,1}$ , node 3, notices the event is triggered. It floods  $f_{2,1}$  in the second relative time slot. Since all other nodes are listening, they receive and forward  $f_{2,1}$ . Different from ST, all nodes keep awake in the first and third relative time slots in case the trigger conditions of  $f_{1,1}$  and  $f_{3,1}$  are violated.

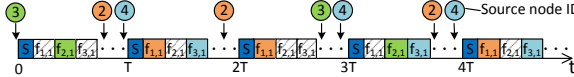


Fig. 7. Event-triggered transmission based on LWB.

5.2.3 *Packet loss recovery for ST.* If all nodes receive  $Tn_i$ , and are synchronized well, they wake up and flood  $f_{i,j}$  at the same time. However, unlike rate adaptation based on LWB, which can self-recover from packet loss, self-triggered transmissions based on LWB are less resilient to packet loss. If a node fails to receive  $Tn_i$ , it is possible that it will not wake up at the right time for the next transmission and will become unsynchronized with other nodes for  $f_{i,j}$  forever. Table 3 shows an example of the impact of packet loss on flow  $f_{1,1}$ , when a holistic controller predicts a series of inter-transmission intervals ( $Tn_1$ ).  $\{1, 0, /\}$  in brackets following  $Tn_1$  indicate that the node receives a packet, loses a packet, and remains sleeping, separately, correspond to its inter-transmission interval  $Tn_1$ . In this example, the update inter-transmission time  $Tn_1 = T$  is received by nodes 2 and 3, but fails to arrive at node 4 in first period ( $t_{1,1}$ ) due to packet loss. Hence, the nodes 2 and 3 schedule next transmissions in the second period ( $t_{1,1} + T$ ), while node 4 uses last  $Tn_1 = 2T$  and schedules next transmission in the third period ( $t_{1,1} + 2T$ ). In the second period, nodes 2 and 3 receive new  $Tn_1 = 2T$ , and schedule the next transmissions in the fourth period ( $t_{1,1} + 3T$ ). Node 4 sleeps at this period and loses the updated inter-transmission time again. If the system goes on like this, node 4 becomes unsynchronized with other nodes and loses all packets. Therefore, it is of vital importance to come up with effective and efficient strategies to recover from packet loss. We propose the following packet loss recovery strategy: if a node wakes up but does not receive a packet with  $Tn_i$ , it should re-awake at the highest rate  $R$ , until another packet with  $Tn_i$  is received.

## 6 REAL-TIME WCPS

To experiment with wireless control over real-world WSA<sub>N</sub>s, we develop a real-time wireless cyber-physical simulator (RT-WCPS). In this section, we first present the architecture of RT-WCPS. Then we analyze its real-time performance.

### 6.1 Architecture of RT-WCPS

RT-WCPS integrates *MATLAB/Simulink Desktop Real-time (SLDRT)* [52] and a *3-floor WSA<sub>N</sub> testbed* [53, 54]. The architecture of RT-WCPS is shown in Fig. 8. Note that this figure shows the architecture of one wireless control loop. Several control loops can share the same WSA<sub>N</sub>.

SLDRT is used to simulate the physical part of the WNC<sub>S</sub>: physical plants, controllers, state observers, and physical disturbance. In practice, industrial plants usually operate continuously or at very high rates. However, the wireless communication and controller execute at a relatively low rate because of the communication and computation latencies. Therefore, SLDRT modules are operated at different rates in our design.



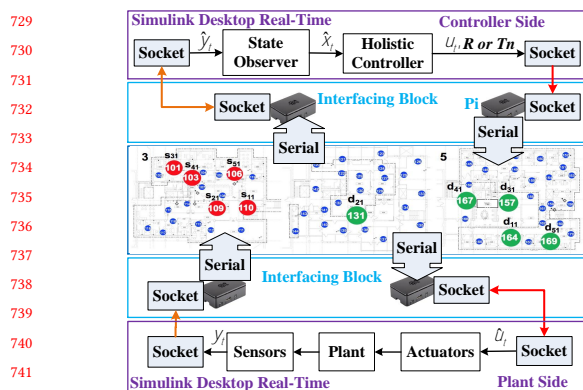


Fig. 8. Architecture of RT-WCPS.

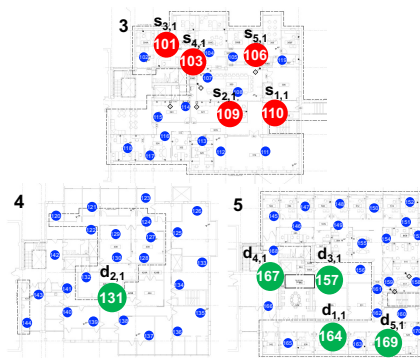


Fig. 9. 3-floor WSAW testbed in Jolley Hall of Washington University in St. Louis (from left to right, third floor to fifth floor).

The 3-floor WSAW testbed is deployed on the 3rd to 5th floors of Jolley Hall at Washington University in St. Louis, as shown in Fig. 9. It consists of 70 TelosB motes. Each mote is equipped with Chipcon CC2420 radio compliant with the IEEE 802.15.4 standard and a TI MSP430 microcontroller. 40 Raspberry Pis with a backplane network are used for the measurement and management of the wireless network [6].

The interfaces between SLDRT and WSAW are socket connections between the PCs that run SLDRT and the Pis, and serial connections between the Pis and the end nodes. In this way, the end nodes  $s_{i,j}, d_{i,j}$  of the sensing and actuation flows  $f_{i,j}$  can be any nodes in the testbed.

## 6.2 Real-time network-in-the-loop simulation

Both SLDRT and the 3-floor WSAW testbed operate in real-time. To evaluate the real-time performance of the RT-WCPS, we measure the latency caused by each module. In our design, sensing and actuation flows have the same overhead induced by interfaces, since they have the same types of interfaces between physical parts and WSAW as in Fig. 8, and all data flows share the same WSAW with independent interfaces.

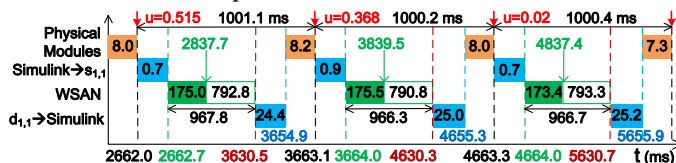


Fig. 10. Timeline of RT-WCPS

We use the latencies of one actuation flow as an illustrative example. First, we adopt the *Precision Time Protocol* (PTP) to synchronize the PC that runs SLDRT and the Pis. PTP is a protocol used to synchronize clocks throughout a network. It achieves clock accuracy in the sub-microsecond range [55]. Then, we record the completion timestamps of each module on corresponding machines (1) the physical modules, (2) the actuation flow from Simulink to  $s_{1,1}$ , (3) the transmissions in WSAW, (4) the actuation flow from  $d_{1,1}$  to Simulink. Finally, we draw the timeline of RT-WCPS and analyze the latencies, as shown in Fig. 10. We set the sampling period to 1s, which is the fastest update time supported by most industrial WSAW products. From the timeline, the total overhead induced by interfaces between Simulink and the node is less than 26 ms (2.6%). More than 966 ms is reserved for communication over the WSAW in each period, among which around 175 ms is utilized for transmissions in this example. The results validate the real-time performance of RT-WCPS. Please note that 26 ms overhead is acceptable when we use RT-WCPS to simulate industrial processes like oil refinery and mining, sampling periods of which are usually longer than 1 s [38]. However, it is not acceptable

781 in faster sampling period of tens of milliseconds. We will work on shortening this overhead in the future. We refer  
 782 interested readers to [15, 32, 39] for network and WNCs designs with tighter time requirements.  
 783

## 784 7 EVALUATION

785  
 786 In this section, we describe systematic trials of our wireless control designs using RT-WCPS. On the physical side, to  
 787 represent an industrial process system, we use up to five 4-state load positioning systems that share the same WSN.  
 788 On the WSN side, we evaluate the proposed network protocols over a 70-node WSN testbed [53, 54].  
 789

790 Because the state observer provides robust and theoretically sound protection against loss of sensing information [7, 56,  
 791 57], the WNCs are more sensitive to packet loss on the actuation side of WSN [21]. Thus, we focus on comprehensive  
 792 actuation-network-in-the-loop simulations. We then empirically evaluate the tradeoff between rate adaptation (RA)  
 793 and self-triggered control (ST) in communication cost and control performance under different operating conditions.  
 794

### 795 7.1 Systems settings

796  
 797 **7.1.1 Physical system settings.** We run simulations of a realistic load positioning system [58, 59], which positions a  
 798 load (L) using a motor with a ballscrew transmission. The motor is attached rigidly to a movable base platform (B). The  
 799 load positioning is a 4-state nonlinear system as described in [59]. When the system is operated at low rates as in real  
 800 industrial applications, the stiffness of the ballscrew and the potential energy stored in it are neglected in the model.  
 801 The system can be simplified as a 4-state linear system [58]:  
 802  
 803

$$804 \dot{x}_t = A_c x_t + B_c u_t, y_t = C_c x_t, \quad (20)$$

805 where

$$806 A_c = \begin{bmatrix} 0 & 1 & 0 & 0 \\ 0 & -d_L(\frac{1}{m_L} + \frac{1}{m_B}) & \frac{k_B}{m_B} & \frac{d_B}{m_B} \\ 0 & 0 & 0 & 1 \\ 0 & \frac{d_L}{m_B} & -\frac{k_B}{m_B} & -\frac{d_B}{m_B} \end{bmatrix}, B_c = \begin{bmatrix} 0 \\ \frac{1}{m_L} + \frac{1}{m_B} \\ 0 \\ -\frac{1}{m_B} \end{bmatrix},$$

807 and  $C_c = [1 \ 0 \ 0 \ 0]$ . Here,  $d_L$ ,  $m_L$ ,  $d_B$ ,  $m_B$ , and  $k_B$  are parameters of the load and base platforms, such as the  
 808 mass, damping, and stiffness. The state vector is defined as  $x_t = [x_L(t) \ \dot{x}_L(t) \ x_B(t) \ \dot{x}_B(t)]^T$ , where  $x_L$  is the displacement  
 809 of the load *relative* to the base platform,  $x_B$  is the *absolute* displacement of the base platform, and  $\dot{x}_L$  and  $\dot{x}_B$  are the  
 810 speeds of the relative and absolute movements. We will stabilize the states of the load positioning system to the origin.  
 811

812 There are two kinds of plants. For the first kind, denoted as PLANT1,  $d_L = 15$ ,  $m_L = 100$ ,  $d_B = 10$ ,  $m_B = 10$ ,  
 813  $k_B = 5$ , and  $K = [-1.9393 \ -13.1373 \ 0.0842 \ -13.0264]$ . For the second kind, denoted as PLANT2,  $d_L = 10$ ,  $m_L = 15$ ,  
 814  $d_B = 3$ ,  $m_B = 5$ ,  $k_B = 2$ , and  $K = [-1.0076 \ -0.6317 \ -0.1954 \ -0.3814]$ . The second kind of plants have lower mass  
 815 and damping, therefore their response time is shorter than that of PLANT1. In holistic controller, we discretize the  
 816 continuous-time models (20) using *step-invariant transformation* at its corresponding sampling period  $T_i$ :  
 817  $A_{T_i} = e^{A_c T_i}$ ,  $B_{T_i} = \int_0^{T_i} e^{A_c \tau} d\tau B_c$ .  
 818

819 For each control loop, given the discrete-time model,  $K$ , and  $Q$ , we can get  $P$ ,  $\alpha_1$ ,  $\alpha_2$ , and  $\beta$  according to (16), (5), and  
 820 (6), respectively. For all loops,  $Q = I_4$ ,  $W_Q = I_4$ ,  $W_R = 1$ ,  $\gamma = 1$ , and  $\delta = 2$ . We will adjust and evaluate some parameter  
 821 selections of RA, such as  $V_{Ith}$ ,  $\lambda$  and  $\tau$  of heuristic RA algorithm, and  $\epsilon_2$  of the optimal RA problem.  
 822  
 823

824  
 825 **7.1.2 WSN settings.** The network protocols for RA and ST use Contiki [60]. The LWB operates at the rate  $R = 1$  Hz.  
 826 The global static schedule has one synchronization slot, with a length of 25 ms, and 2-5 data slots, with lengths of 18 ms.  
 827  
 828

70 nodes participate in the transmissions. The synchronization packet is disseminated by the sink node (node 164) every 1 s. The synchronization packet size is 6 bytes, and the data packets are 25 bytes. Each data slot is used to transmit the control command  $u_t$  and network reconfiguration signals  $R$  or  $Tn$  of each control loop. Fig. 9 shows the source and destination pairs of five actuation flows over 3-floor WSAN. The Tx power is 0 dbm, and the retransmission number is 3.

**7.1.3 RT-WCPS settings.** We simulate the WNCSSs using RT-WCPS, which integrates a 70-node WSAN and SLDRT. We simulated two control loops sharing a WSAN for statistical results from Sec. 7.3 to Sec. 7.6. Loop  $l_1$  controls a PLANT1. Loop  $l_2$  controls a PLANT2. The SLDRT modules of two loops are shown in Fig. 11. Each loop has its own holistic controller, and the controllers and the actuators communicate via actuation flows sharing the same WSAN. And we simulate five control loops sharing a WSAN to show the scalability of RT-WCPS in Sec. 7.7. Loops  $l_1$ ,  $l_3$ , and  $l_5$  control 3 PLANT1s separately. Loops  $l_2$  and  $l_4$  control 2 PLANT2s.

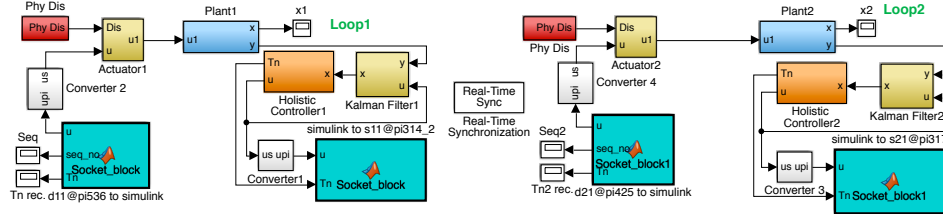


Fig. 11. SLDRT modules of RT-WCPS.

As presented in Sec. 6.1, modules in Fig. 11 operate at different rates. The physical plants run at 100 Hz. Kalman filters and actuators run at 1 Hz. The “worst-case-guaranteed” WSAN and controllers run at 1 Hz, and WSAN and controllers can adjust their rates and operate ST during runtime, based on control needs. In RA, we choose candidate rates: 1 Hz, 0.5 Hz, 0.25 Hz, which are reasonable rates for our load positioning systems with time constants of roughly 30 s. And they are also typical rates in industrial process control [38]. In order to provide robustness guarantees of the self-triggered control [11], we set the upper bound of the inter-transmission interval as 10 s.

## 7.2 Evaluation of optimal and heuristic rate adaptation algorithms

We first evaluate the optimal and heuristic RA algorithms. Since they are control designs, we temporarily run simulations under ideal network (100% packet delivery ratio and no latency) in Sec. 7.2. We then run network-in-the-loop simulations with different holistic control approaches under different physical and network conditions in Secs. 7.3-7.7.

**7.2.1 Heuristic rate adaptation.** We first evaluate the online heuristic RA. Fig. 12 shows how heuristic RA works. Take PLANT1 as an example. We introduce physical disturbance by injecting a constant bias into the actuator from 120 to 140 s, as shown in plot (a). Plot (b) shows the Lyapunov function  $V(x_t)$ . The two dashed lines, from upper to lower, are the thresholds for increase and decrease of rate. Plot (c) shows the sampling rate adaptation.  $Tn$  indicates the time till the next packet Tx, i.e., sampling period in RA. Plots (d) and (e) show the control command  $u_t$  and physical states  $x_t$ , respectively. During the transient (0 – 60 s and 120 – 160 s), the control performance is poor, which is reflected by a large value of  $V(x_t)$ . When  $V(x_t)$  is above the increase threshold, the holistic controller increases the rate. When  $x$  is approaching the origin (80 – 120 s and 170 – 200 s), as indicated by the decreases of  $V(x_t)$ , and  $V(x_t)$  is below the decrease threshold for  $\tau = 10$  s, the rate of the WSAN decreases shown in (c).

Fig. 13 shows the impact of parameter tuning in heuristic rate selection, i.e., the increased threshold  $V_{Ith}$ , decreased threshold coefficient  $\lambda$ , and the test time interval  $\tau$ . Each marker in this figure is obtained by carrying out 20 rounds of simulations. We use the mean absolute error (MAE) as the metric of control performance, and the number of

885  
886  
887  
888  
889  
890  
891  
892  
893  
894  
895  
896  
897

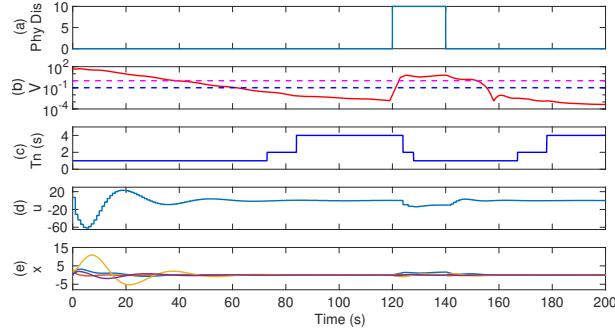
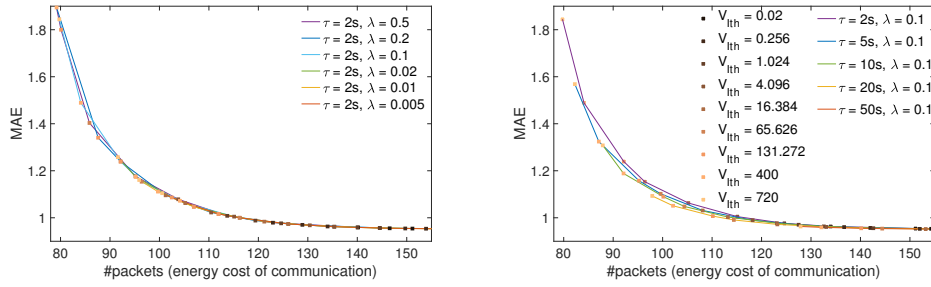


Fig. 12. Response curve of heuristic rate adaptation

898  
899  
900  
901  
902  
903  
904  
905  
906  
907

packets sent through WSA as the metric of energy cost. The value of X-axis is the mean of MAEs in 20 rounds of simulations, and the value of Y-axis is the mean of total number of packets. As described in Sec. 4.1.1,  $V_{Ith} = \alpha_1 \|x_{se}\|^2$ ,  $V_{Dth} = \lambda \alpha_1 \|x_{se}\|^2$ . Thus, the intuition is that smaller  $V_{Ith}$  makes rate increase more often, and smaller  $\lambda$  and longer  $\tau$  make rate decrease less often. We can see that with fixed  $\tau$  and  $\lambda$ , the MAE decreases at the cost of more network energy consumption as  $V_{Ith}$  becomes smaller. There is a diminishing return of control performance improving as increase of energy cost. Fig. 13A shows that  $\lambda$  mostly does not affect the trajectory of curves, which indicate relationship between MAE and network energy cost. With fixed  $V_{Ith}$  and  $\tau$ , MAE decreases at more energy cost when  $\lambda$  is smaller. The same impact holds for  $\tau$  in Fig. 13B that MAE decreases at more energy cost when  $\tau$  is longer.

908  
909  
910  
911  
912  
913  
914  
915  
916  
917



(A) Various  $\lambda$

(B) Various test interval  $\tau$

Fig. 13. Impacts of parameters in heuristic rate selection.

920  
921  
922  
923  
924  
925  
926  
927  
928  
929  
930  
931  
932

**7.2.2 Optimal rate selection.** We evaluate the optimal rate selection. Fig. 14 shows how optimal rate selection works. Plot (b) shows the values of objective function  $\mathcal{J}$  of three candidate rates and the optimal rate solution of the optimization problem (15). During the transient processes around 0 – 50 s and 125 – 150 s, the control performance dominates  $\mathcal{J}$ . Therefore high sampling rate minimizes  $\mathcal{J}$ . While when the system is stable during 80 – 120 s and 180 – 200 s, the communication cost dominates  $\mathcal{J}$ . Thus low rate minimizes  $\mathcal{J}$ . In this way, optimal rate selection facilitates a systematic balance between energy cost and control performance through adjusting the weight ( $\epsilon_2$ ) in  $\mathcal{J}$ . Fig. 15 shows the relationship between MAE, communication cost, and  $\epsilon_2$ . Each marker is obtained by 20 rounds of simulations. Larger  $\epsilon_2$  reduces energy cost at the cost of control performance and *vice versa*. Considering the diminishing return of MAE improvement, proper  $\epsilon_2$  could be chosen to achieve small MAE at the cost of reasonable network energy cost.

933  
934  
935  
936

**7.2.3 Comparison between optimal and heuristic approaches.** The optimal rate selection is able to systematically balance energy and control performance. It does not need any threshold compared to heuristic rate selection. However, since

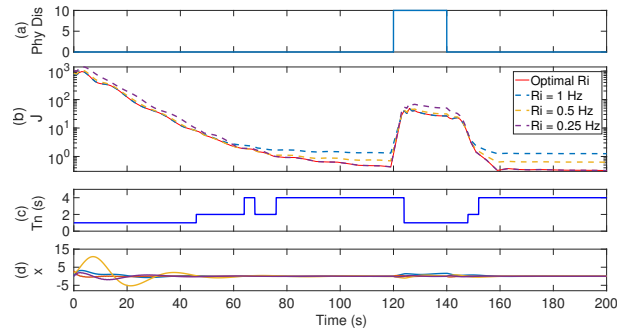


Fig. 14. Response curve of optimal rate adaptation

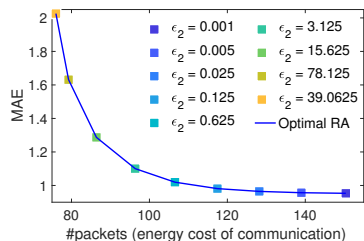
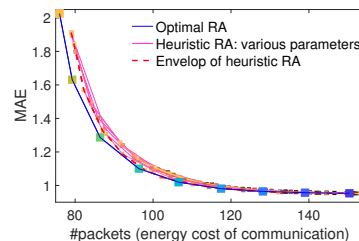
Fig. 15. Impact of  $\epsilon_2$  in optimal rate adaptation.

Fig. 16. Compare optimal rate selection and heuristic RA.

we propose to adapt the rate at run-time, computational complexity of the algorithms matters. Optimal rate selection problem is an integer programming problem. Its computational complexity is higher than the heuristic approach with the complexity of  $O(1)$ . Fig. 16 compares the performance of optimal and heuristic RA approaches. The markers on the lower left of the figure indicate better performance that can achieve smaller MAE with less energy cost. We can see that the optimal rate selection has slightly better performance than the best envelop of the heuristic approach. The envelop is achieved by arbitrarily tuning combinations of parameters 90 times as shown in Fig. 13. On the other hand, tuning  $\epsilon_2$  in optimal RA is more efficient to balance energy and control performance. However, we can also see that the advantage of optimal rate selection is less remarkable when the requirement of control performance is stringent, as shown in the right bottom part of Fig. 16. Since we have a specific and stringent requirement on control performance, i.e.,  $\|x_{se}\|^2 = 0.1$ ,  $\lambda = 0.1$  and  $\tau = 10$  s, we choose to adopt heuristic rate selection in the rest of sections.

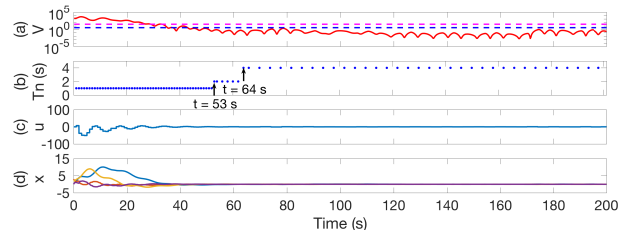
### 7.3 Normal network and physical conditions

We then run network-in-the-loop simulations. We evaluate the WNCSS under normal conditions. The WSAN operated on IEEE 802.15.4's channel 26. The average packet delivery ratio is 99.15%. And there is no physical disturbance. We present the results of five sets of network-in-the-loop simulations under the different management approaches:

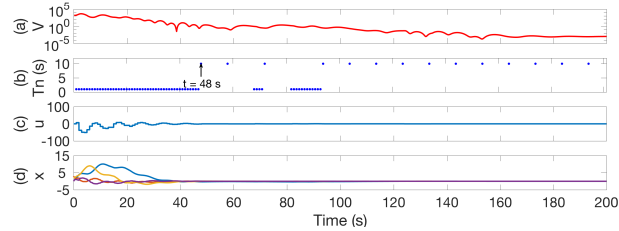
(1) RA: Fig. 17A shows the response curves of loop 1. In plot (b), each dot indicates Tx of one packet, and the y-axis of the dot is the time till the next Tx. When  $x$  is approaching the origin, as indicated by the decreases of  $V(x_t)$ , and  $V(x_t)$  is below the decrease threshold for  $\tau = 10$  s, the rate of the WSAN starts to decrease, as shown in (b). The rate changes from 1 Hz (1 Tx every 1 s), to 0.5 Hz (1 Tx every 2 s) at  $t = 53$  s, then to 0.25 Hz (1 Tx every 4 s) at  $t = 64$  s.

(2) ST: Fig. 17B shows the response curve of ST. In (b), since  $V(x_t)$  decreases, the inter-transmission interval changes from 1 s to 10 s at  $t = 48$  s. When  $V(x_t)$  increases at around 60 s to 90 s,  $T_n$  reduces to 1 s as soon as the timer expires.

(3) Fixed rate time-driven control: Existing WSANs typically employ time-drive transmissions with fixed rates, so we use three fixed rates of 1 Hz, 0.5 Hz and 0.25 Hz, denoted by 1, 2, 4 in following statistical results.



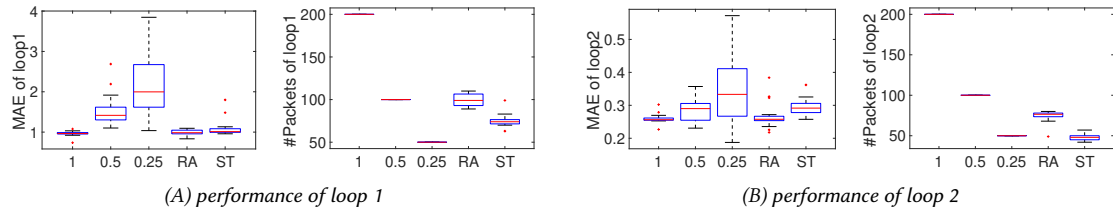
(A) time-driven control with rate adaptation



(B) self-triggered control

Fig. 17. Response curve under normal condition.

Next we run each experiment for 20 rounds with different initial values to statistically compare different approaches. Fig. 18 shows the performances of two loops. Both RA and ST can achieve similar control performances with fixed rate of 1 Hz, with a network cost (# of packets) reduction of more than 50%. Loop 2 has network cost reduction of more than 62%, since it has shorter time constant. For both loops, ST is more aggressive in saving network cost than RA.



(A) performance of loop 1

(B) performance of loop 2

Fig. 18. Performance under normal condition.

In reality, the total energy cost of all flows, including the synchronization cost, is of interest. Therefore, we analyze power cost over the WSAN in detail. We collect the time spent in transmitting and listening per node per second using the Energest module [61] provided by Contiki OS. The sum of transmitting and listening time is the radio-on time of the collection period, and the node sleeps in the rest of the period. We adopt the energy model in [62] to estimate the energy cost. Fig. 19A and Fig. 19B show that the energy cost are consistent with duty cycle. Fig. 19A shows the average energy cost of all 70 nodes is consistent with the number of packets going through WSAN. RA and ST save 40% energy, which is higher than energy cost of loop1 and loop2 alone in Fig. 18, since energy estimation includes the cost of synchronization every second. However, in the case of the maximum energy cost, ST costs more than RA, which can be explained by the fact that the node incurs the maximum energy cost due to packet loss. Facing packet loss, the node with the ST transmissions protocol keeps listening at a high energy cost because of its recovery mechanism. Whereas the node with the RA protocol applies self-recovery mechanism without extra energy cost. To verify this difference, we analyze the power cost of two nodes. Node 103 has a higher packet reception ratio than node 124. Fig. 19C shows that ST transmissions are not as efficient as RA for node 124, due to its recovery mechanism. Fig. 20 shows the relationship between MAE and energy cost under normal condition under different management approaches. Each data

point indicates the MAE and energy cost of one round of experiment. Data points of RA and ST are concentrated in the bottom left of the figure, which indicates that those approaches achieve smaller MAE with lower energy cost.

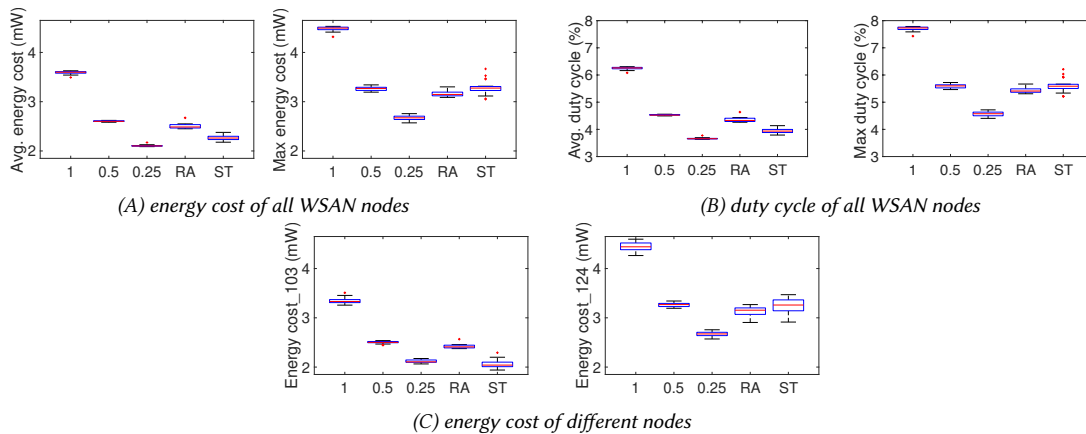


Fig. 19. Energy cost under normal condition.

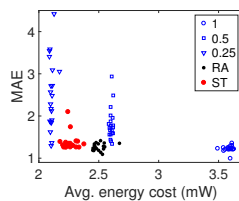


Fig. 20. Relationship between MAE and energy cost under normal condition. The strategies are fixed rate (blue), RA (black), and ST (red).

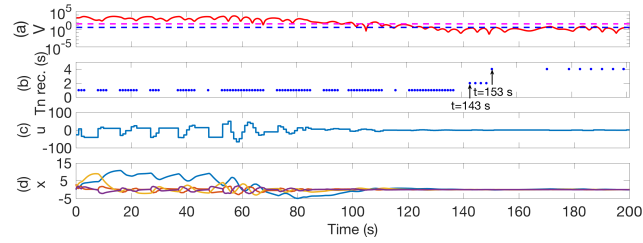
#### 7.4 Network interference

We operate WSA over channel 22 (2.460 GHz) of IEEE.802.15.4, and we introduce network interference by continuously sending jamming packets over an overlapping channel 11 (2.462 GHz) of WiFi. The average packet delivery ratio is reduced to 65.9%. Fig. 21 shows the response curves of RA and ST. In Plot (b), each dot indicates that the actuator receives a packet. Both methods stay longer at high rate than in normal condition to compensate the impact of interferences. And both the network protocols can recover from packet drops. Fig. 22 shows the statistical results under network interference. In this case, both RA and ST guarantee the control performance, at the cost of more energy consumption than Sec. 7.3. ST consumes more energy than RA, due to its packet loss recovery mechanism. Fig. 23 shows the relationship between MAE and energy cost under network interference. Data points of RA and ST are concentrated in the bottom middle, which indicates that those approaches achieve smaller MAE with higher energy cost than normal case due to recovery from network interference, but still lower than 1 Hz sampling. The simultaneous increase of both MAE and energy cost can be explained by the intuition of efficient holistic control that poorer system performance will cause the increase of the rates and number of events. On the other hand, no extra energy is cost when the system is in good condition. This trend indicates that network resources are adapted well based on the states of the physical plants.

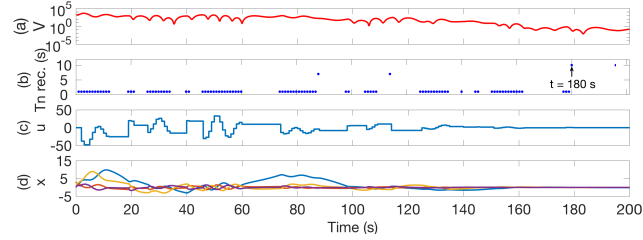
#### 7.5 Physical disturbance

We introduce physical disturbance by adding a constant bias to actuators from 120 s to 140 s. As shown in Fig. 24, both RA and ST adapt rates to 1 Hz under the physical disturbance. However, the time ST ( $t = 130$  s) reacts to the





(A) time-driven control with rate adaptation



(B) self-triggered control

Fig. 21. Response curve under network interference.

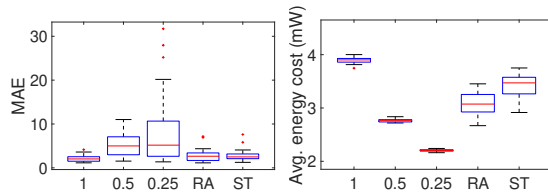


Fig. 22. Performance of double loops under network interference.

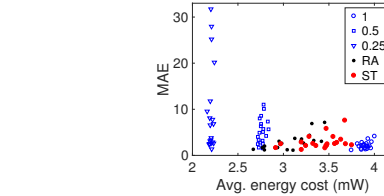


Fig. 23. Relationship between MAE and energy cost under network interference.

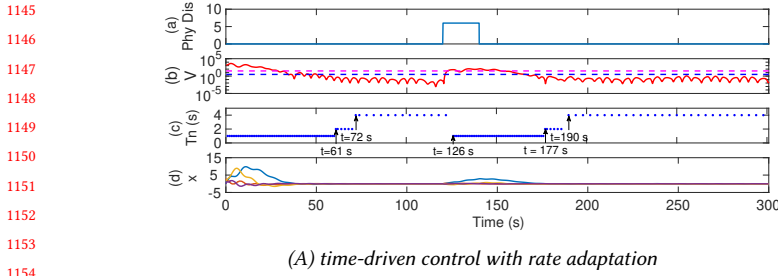
disturbance is later than RA ( $t = 126$  s), since ST has longer  $T_n$  (10 s). Fig. 26 shows the statistical results. As shown in Fig. 26A, both RA and ST have similar MAE with a fixed rate of 1 Hz, and can save more than 30% of the energy. However, as shown in Fig. 26B, the ST performs worse than RA within the interference interval. The longer  $T_n$  (10 s) makes ST response to disturbance slower than time-driven management. Fig. 25 shows the relationship between MAE and energy cost under physical disturbance. Data points of RA and ST are concentrated in the bottom left of the figure, which indicates that those approaches achieve smaller MAE with lower energy cost.

## 7.6 Both network and physical interferences

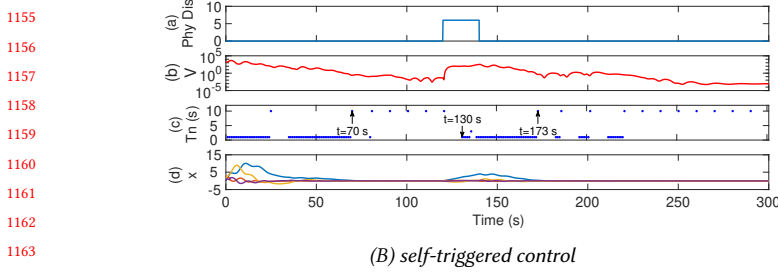
We run experiments with both network and physical interferences in Sec. 7.4 and Sec. 7.5. Fixed rate of 0.25 Hz causes the instability of the system. Therefore, we do not show the results of 0.25 Hz. Fig. 27 shows the statistical results that both RA and ST guarantee the control performance at the costs of more energy consumption than in Sec. 7.5. ST costs more energy than RA, due to the recovery mechanism. Fig. 28 shows the relationship between MAE and energy cost under both network and physical interferences. Data points RA and ST are concentrated in the bottom left, which indicates that those approaches achieve smaller MAE with lower energy cost. The simultaneous increase of both MAE and energy cost indicate that network resources are allocated properly based on the states of the physical plants.

To summarize, in normal physical and network condition, RA and ST can achieve similar control performance to a conventional fixed rate of 1 Hz, while improving energy efficiency. Besides, ST is more aggressive in energy saving





(A) time-driven control with rate adaptation



(B) self-triggered control

Fig. 24. Response curve under physical interference.

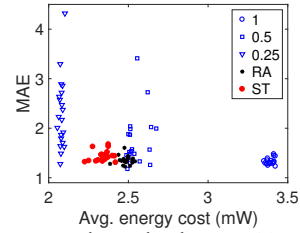
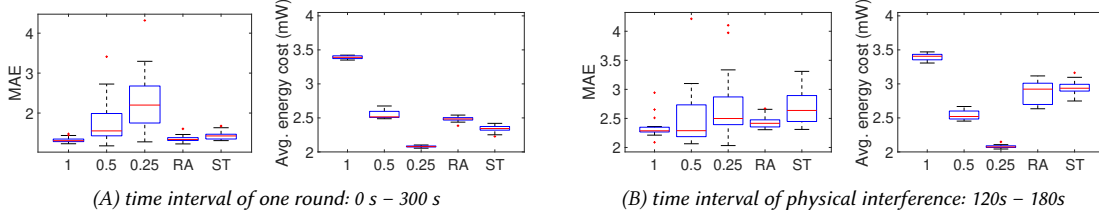


Fig. 25. Relationship between MAE and energy cost under physical disturbance.



(A) time interval of one round: 0 s - 300 s

(B) time interval of physical interference: 120s - 180s

Fig. 26. Performance of double loops under physical interference.

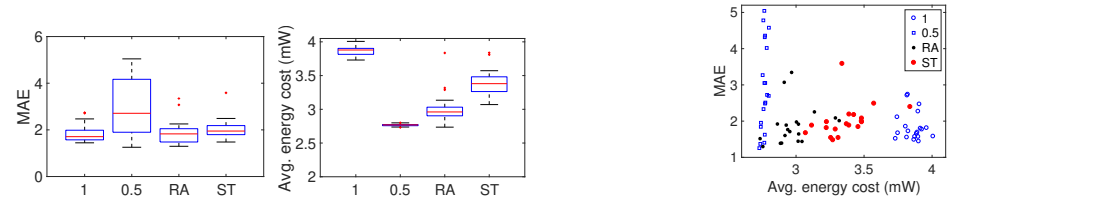


Fig. 27. Performance under network and physical interferences.

Fig. 28. Relationship between MAE and energy cost under both network and physical interferences.

than RA. However, when there are interferences, RA has better performance and energy efficiency than ST, because ST has an embedded recovery mechanism, which costs more energy under packet loss, and a longer inter-transmission interval, which makes ST response slowly to disturbance.

### 7.7 Scalability and flexibility of RT-WCPS

Although above experimental results are based on two control loops. RT-WCPS has the scalability to operate more control loops. In addition, it has the flexibility that end nodes of the data flows can be any nodes in the testbed. As an example, we simulate five control loops sharing a WSA. Loops  $l_1$ ,  $l_3$ , and  $l_5$  control 3 PLANT1s. Loops  $l_2$  and  $l_4$  control 2 PLANT2s. Fig. 9 shows the source and destination pairs of five actuation flows over 3-floor WSA. Table 4 shows the MAEs and energy costs in one round (200 s) of network-in-the-loop simulation under normal condition. Loops  $l_1$ ,  $l_3$ , and  $l_5$  have larger MAEs and are more sensitive to different rates than  $l_2$  and  $l_4$ , since  $l_2$  and  $l_4$  with lower mass and

damping are easier and faster to stabilize. Although there is some randomness in single simulation, it is obvious that RA and ST can achieve similar control performance with fixed rate of 1 Hz, while save energy for more than 47%.

Table 4. Performance of five-loop simulation

	MAE1	MAE2	MAE3	MAE4	MAE5	Energy (mW)
1	0.9666	0.2891	0.9509	0.2292	0.9630	5.2730
2	1.2529	0.3158	1.2800	0.2723	1.6537	3.0461
4	1.5129	0.3131	1.6886	0.2701	1.8859	2.0233
RA	0.9435	0.2623	0.9458	0.2987	0.9671	2.7966
ST	0.9764	0.3148	1.0243	0.3151	0.9943	2.5209

## 8 CONCLUSIONS

Wireless control faces significant challenges due to data loss and energy constraints in WSANs. In this article, we present two efficient holistic control designs for industrial process, rate adaptation (RA) and self-triggered control (ST), that can not only ensure control performance under wireless and physical interferences, but also reduce network energy consumption. Furthermore, we design two network reconfiguration mechanisms based on LWB to support RA and ST in multi-hop WSANs. In addition, we build a real-time network-in-the-loop simulation framework which integrates MATLAB/Simulink and a three-floor WSAN testbed to experiment with wireless control over real-world WSANs. Our empirical studies show that both RA and ST offer advantages in control performance and energy efficiency. The advantage in energy efficiency of ST, however, diminishes under harsh physical and wireless conditions due to the cost of recovering from data loss and physical disturbance.

## REFERENCES

- [1] Pangun Park et al. Wireless network design for control systems: A survey. *IEEE Communications Surveys & Tutorials*, 2018.
- [2] ABB. WirelessHART networks: 7 myths that cloud their consideration for process control Measurement made easy. <https://new.abb.com/products/measurement-products/pl/produkty-i-rozwiazania-wireless/wirelesshart-networks-seven-myths-that-cloud-their-consideration-for-process-control-en>, Retrieved June 21, 2019.
- [3] Emerson™. White paper: Emerson wireless security – WirelessHart and Wi-Fi (2017). <https://www.emerson.com/documents/automation/white-paper-emerson-wireless-security-wirelesshart-wi-fi-security-deltav-en-41260.pdf>, Retrieved June 20, 2019.
- [4] Yehan Ma et al. Holistic cyber-physical management for dependable wireless control systems. *ACM Trans. on Cyber-Physical Systems*, 2018.
- [5] Xiaomin Li et al. A review of industrial wireless networks in the context of industry 4.0. *Wireless networks*, 2017.
- [6] Chenyang Lu et al. Real-time wireless sensor-actuator networks for industrial cyber-physical systems. *Proceedings of the IEEE*, 2016.
- [7] Bruno Sinopoli et al. Kalman filtering with intermittent observations. *IEEE Trans. on Automatic Control*, 2004.
- [8] Manuel Mazo et al. On event-triggered and self-triggered control over sensor/actuator networks. In *IEEE Conference on Decision and Control*, 2008.
- [9] Manuel Mazo et al. Decentralized event-triggered control over wireless sensor/actuator networks. *IEEE Trans. on Automatic Control*, 2011.
- [10] Manuel Mazo Jr et al. An iss self-triggered implementation of linear controllers. *Automatica*, 2010.
- [11] José Araújo et al. System architectures, protocols and algorithms for aperiodic wireless control systems. *IEEE Trans. on Industrial Informatics*, 2014.
- [12] Pangun Park et al. Breath: An adaptive protocol for industrial control applications using wireless sensor networks. *IEEE Trans. Mobile Comput.*, 2011.
- [13] Felix Dobslaw et al. End-to-end reliability-aware scheduling for wireless sensor networks. *IEEE Trans. on Industrial Informatics*, 2016.
- [14] Hyung-Sin Kim et al. Load balancing under heavy traffic in rpl routing protocol for low power and lossy networks. *IEEE Trans. Mobile Comput.*, 2017.
- [15] Marco Zimmerling et al. Adaptive real-time communication for wireless cyber-physical systems. *ACM Trans. on Cyber-Physical Systems*, 2017.
- [16] Zheng Li et al. Adaptive multiple sampling rate scheduling of real-time networked supervisory control system-part ii. In *Annual Conference on IEEE Industrial Electronics*. IEEE, 2006.
- [17] Dip Goswami et al. Time-triggered implementations of mixed-criticality automotive software. In *Proceedings of the Conference on Design, Automation and Test in Europe*. EDA Consortium, 2012.
- [18] Burak Demirel et al. Modular design of jointly optimal controllers and forwarding policies for wireless control. *IEEE Trans. Autom. Control*, 2014.
- [19] Abusayeed Saifullah et al. Near optimal rate selection for wireless control systems. *ACM Trans. on Embedded Computing Systems*, 2014.
- [20] Dohwan Kim et al. Sampling rate optimization for iec 802.11 wireless control systems. In *International Conference on Cyber-Physical Systems*, 2019.
- [21] Bo Li et al. Wireless routing and control: a cyber-physical case study. In *ACM/IEEE International Conference on Cyber-Physical Systems*. IEEE, 2016.
- [22] Jia Bai et al. Optimal cross-layer design of sampling rate adaptation and network scheduling for wireless networked control systems. In *IEEE/ACM International Conference on Cyber-Physical Systems*. IEEE, 2012.

- 1249 [23] Lei Bao et al. Rate allocation for quantized control over noisy channels. In *International Symposium on Modeling and Optimization in Mobile, Ad Hoc,*  
1250 *and Wireless Networks*. IEEE, 2009.
- 1251 [24] J Colandairaj et al. Wireless networked control systems with qos-based sampling. *IET Control Theory & Applications*, 2007.
- 1252 [25] Anton Cervin et al. How does control timing affect performance? analysis and simulation of timing using jitterbug and truetime. *IEEE control*  
1253 *systems*, 2003.
- 1254 [26] Emeka Eyisi et al. Ncswt: An integrated modeling and simulation tool for networked control systems. *Simulation Modelling Practice and Theory*,  
1255 2012.
- 1256 [27] Kannan Srinivasan et al. An empirical study of low-power wireless. *ACM Trans. on Sensor Networks*, 2010.
- 1257 [28] Carlos Santos et al. Aperiodic linear networked control considering variable channel delays: Application to robots coordination. *Sensors*, 2015.
- 1258 [29] Bo Li et al. Incorporating emergency alarms in reliable wireless process control. In *International Conference on Cyber-Physical Systems*. ACM, 2015.
- 1259 [30] Philip Levis et al. Tossim: Accurate and scalable simulation of entire tinyos applications. In *International Conference on Embedded Networked Sensor*  
*Systems*. ACM, 2003.
- 1260 [31] Miroslav Pajic et al. Closing the loop: A simple distributed method for control over wireless networks. In *ACM/IEEE International Conference on*  
1261 *Information Processing in Sensor Networks*. IEEE, 2012.
- 1262 [32] Fabian Mager et al. Feedback control goes wireless: Guaranteed stability over low-power multi-hop networks. In *ACM/IEEE International Conference*  
1263 *on Cyber-Physical Systems*. ACM, 2019.
- 1264 [33] Dominik Baumann et al. Evaluating low-power wireless cyber-physical systems. In *IEEE Workshop on Benchmarking Cyber-Physical Networks and*  
1265 *Systems*. IEEE, 2018.
- 1266 [34] Dominik Baumann et al. Control-guided communication: Efficient resource arbitration and allocation in multi-hop wireless control systems. *IEEE*  
*Control Systems Letters*, 2019.
- 1267 [35] Kemin Zhou et al. *Robust and optimal control*. Prentice hall New Jersey, 1996.
- 1268 [36] Federico Ferrari et al. Low-power wireless bus. In *ACM Conference on Embedded Network Sensor Systems*. ACM, 2012.
- 1269 [37] Federico Ferrari et al. Efficient network flooding and time synchronization with glossy. In *International Conference on Information Processing in*  
1270 *Sensor Networks*. IEEE, 2011.
- 1271 [38] Gang Zhao. Wireless sensor networks for industrial process monitoring and control: A survey. *Network Protocols and Algorithms*, 2011.
- 1272 [39] Timofei Istomin et al. Data prediction+ synchronous transmissions= ultra-low power wireless sensor networks. In *ACM Conference on Embedded*  
1273 *Network Sensor Systems*. ACM, 2016.
- 1274 [40] Tongwen Chen et al. *Optimal sampled-data control systems*. Springer Science & Business Media, 2012.
- 1275 [41] Bruce Francis. The optimal linear-quadratic time-invariant regulator with cheap control. *IEEE Trans. on Automatic Control*, 1979.
- 1276 [42] Hai Lin et al. Stability and stabilizability of switched linear systems: a survey of recent results. *IEEE Trans. on Automatic control*, 2009.
- 1277 [43] Wei Zhang et al. Stability of networked control systems. *IEEE Control Systems*, 2001.
- 1278 [44] Huijun Gao et al. A new delay system approach to network-based control. *Automatica*, 2008.
- 1279 [45] Merid Lješanjanin et al. Packetized mpc with dynamic scheduling constraints and bounded packet dropouts. *Automatica*, 2014.
- 1280 [46] Jing Wu et al. Design of networked control systems with packet dropouts. *IEEE Trans. on Automatic Control*, 2007.
- 1281 [47] Jamal Daafouz et al. Stability analysis and control synthesis for switched systems: a switched lyapunov function approach. *IEEE Trans. on Automatic*  
*Control*, 2002.
- 1282 [48] Daniel Liberzon et al. Basic problems in stability and design of switched systems. *IEEE control systems magazine*, 1999.
- 1283 [49] S-H Lee et al. A new stability analysis of switched systems. *Automatica*, 2000.
- 1284 [50] Dragan Nesić et al. Input-output stability properties of networked control systems. *IEEE Trans. on Automatic Control*, 2004.
- 1285 [51] Bin Hu et al. Co-design of safe and efficient networked control systems in factory automation with state-dependent wireless fading channels.  
1286 *Automatica*, 2019.
- 1287 [52] Simulink. Simulink Desktop Real-Time. <https://www.mathworks.com/products/simulink-desktop-real-time.html>, Retrieved December 12, 2018.
- 1288 [53] Mo Sha et al. Implementation and experimentation of industrial wireless sensor-actuator network protocols. In *European Conference on Wireless*  
*Sensor Networks*. Springer, 2015.
- 1289 [54] Mo Sha et al. Empirical study and enhancements of industrial wireless sensor-actuator network protocols. *IEEE Internet of Things Journal*, 2017.
- 1290 [55] PTP. PTP protocol, Retrieved December 12, 2018. <https://www.nist.gov/el/intelligent-systems-division-73500/ieee-1588>.
- 1291 [56] Xiangheng Liu et al. Kalman filtering with partial observation losses. In *IEEE Conference on Decision and Control*. IEEE, 2004.
- 1292 [57] Yang Shi et al. Kalman filter-based identification for systems with randomly missing measurements in a network environment. *International Journal*  
1293 *of Control*, 2010.
- 1294 [58] Vijay Shilpiekandula et al. Load positioning in the presence of base vibrations. In *American Control Conference*. IEEE, 2012.
- 1295 [59] Yu Jiang et al. Optimal codesign of nonlinear control systems based on a modified policy iteration method. *IEEE Trans on Neural Networks and*  
1296 *Learning Systems*, 2015.
- 1297 [60] Chayan Sarkar. Lwb and fs-lwb implementation for sky platform using contiki. *arXiv preprint arXiv:1607.06622*, 2016.
- 1298 [61] Adam Dunkels et al. Software-based on-line energy estimation for sensor nodes. In *Workshop on Embedded Networked Sensors*. ACM, 2007.
- 1299 [62] Chengjie Wu et al. Maximizing network lifetime of wireless networks under graph routing. In *IEEE International Conference on Internet-of-Things*  
*Design and Implementation*, 2016.